Master's thesis

Master's Programme in Particle Physics and Astrophysical Sciences

Percolation of Bubbles in a Cosmological Phase Transition

Lasse Sihvonen

July 29, 2025

Supervisor(s): Prof. Mark Hindmarsh

Examiner(s): Prof. Mark Hindmarsh
Prof. Kari Rummukainen

University of Helsinki
Faculty of Science

P. O. Box 68 (Pietari Kalmin katu 5)
00014 University of Helsinki

HELSINGIN YLIOPISTO — HELSINGFORS UNIVERSITET — UNIVERSITY OF HELSINKI

Tiedekunta — Fakultet — Faculty	Koulutusohjelma — Utbildningsprogram — Degree programme
Faculty of Science	Master's Programme in Particle Physics and Astrophysical Sciences

Tekijä — Författare — Author

Lasse Sihvonen

Työn nimi — Arbetets titel — Title

Percolation of Bubbles in a Cosmological Phase Transition

Työn laji — Arbetets art — Level	Aika — Datum — Month and year	Sivumäärä — Sidantal — Number of pages
Master's thesis	July 29, 2025	61

Tiivistelmä — Referat — Abstract

Cosmological phase transitions have seen a resurgence of interest as a research topic due to the possibility of detecting gravitational waves (GWs) with the upcoming Laser Interferometer Space Antenna (LISA) from such an event. This would give us a way of looking into the early Universe, as a phase transition would likely have occurred during the very early Universe before the Cosmic Microwave Background. Currently, a likely candidate for the source of GWs would be a first-order phase transition at the electroweak (EW) scale $T \approx 100$–1000 GeV. Measuring the GW spectrum and comparing it against theory could give us information about physics beyond the Standard Model (SM).

A first-order phase transition proceeds via nucleation of bubbles of the new phase. In the context of a cosmological phase transition at the EW scale, the new phase represents a configuration of the quantum field where certain symmetries are broken. As these bubbles nucleate, they grow and form connected regions of space called clusters. When an infinite cluster is formed, it is said that the system percolates. The formation of such a cluster is often a critical phenomenon, such that there is some critical fraction of bubbles ϕ_c that is required for percolation to occur.

In this thesis, we study the phenomenon of percolation in the context of cosmological phase transitions. We develop a simulation method using `Fortran` to estimate the critical fraction ϕ_c for two different phase transitions; a fast transition with exponential bubble nucleation and a slow transition, where the barrier between the phases persists down to zero temperature. We compare the results against the commonly used approximation of using the uniformly distributed equal-size sphere ϕ_c in a cosmological phase transition. We find relatively good evidence that the use of such an approximation underestimates ϕ_c in both scenarios.

Avainsanat — Nyckelord — Keywords

phase transitions, percolation, early universe

Säilytyspaikka — Förvaringsställe — Where deposited

Muita tietoja — Övriga uppgifter — Additional information

Contents

1. Introduction

The Laser Interferometer Space Antenna (LISA) is set to launch in the next decade with the goal of measuring gravitational waves [1, 2]. Some of these gravitational waves (GWs) that could be measured with LISA could potentially have been generated from a first-order cosmological phase transition in the early Universe at the electroweak (EW) scale, around $\sim 10^{-11}$ s after the big bang [3–5]. Detecting such GWs with LISA could give us a peek into physics beyond the Standard Model (SM), as it predicts a transition[†] that would not source GWs. Another motivation to study the first-order phase transition at the EW scale is to explain the matter-antimatter asymmetry via baryogenesis [3]. We will not cover baryogenesis in this thesis and refer the reader to an introduction to the topic which can be found in [6].

During a cosmological phase transition the underlying quantum field, the Higgs field, as described by underlying particle physics, transitions from a symmetric phase to a symmetry-broken phase. The nature of this transition depends on the shape of the potential of the field, and as such the resulting GW spectrum is dependent on the fundamental particle physics at a microscopic scale, and different extensions of the SM can give different predictions for the spectrum of GWs. There are three main contributions to the GW spectrum; collision of the bubble walls, sound waves, and turbulence in the plasma [3, 5].

A first-order phase transition proceeds via nucleation of bubbles of a new phase. As these bubbles grow, they fill a larger portion of space until in an ideal transition the whole system is in the new phase. One of the necessary conditions for this to occur is the formation of an infinite connected cluster of bubbles. The formation of this infinite cluster is called *percolation*. Percolation can be illustrated by the movement of fluid through a porous material: a system percolates when we can move across the whole volume through the pores of the material, for example, water trickling coffee grounds. The main goal of this thesis is to simulate the nucleation of bubbles to find the critical fractional volumes ϕ_c that the bubbles must take up for percolation to occur. Although its significance is minor for fast transitions, in a strongly supercooled phase transition it is often used as a milestone to predict GW production [5].

[†]A cross-over which some do not consider a phase transition.

In this thesis, we will look at two specific cases of a first-order phase transition, one which we call a *slow* transition and the other a *fast* transition. The former is the scenario where the Universe remains supercooled down to zero-temperature, such that the nucleation rate tends towards a constant value per physical volume, and we cannot neglect the expansion of the Universe. This closely follows the graceful exit problem in [7], which was the original proposal for the inflation mechanism. In the fast transition scenario, we assume an exponential nucleation rate and that the transition is fast enough so that we can ignore the effect of expansion.

The outline of the thesis is as follows. In Section 2 we introduce some of the theoretical background of cosmological phase transitions with a focus on the first-order phase transitions and cover the two specific cases of a phase transition. In Section 2.2.3 we cover some basic percolation theory and its relation to the phase transition and our methodology used to determine the critical fractional volume ϕ_c. Section 3 focuses on the simulation methods we use to study percolation and in Section 4 we cover some details about the simulation and how we test it for a case of uniformly distributed equal-sized spheres for which the value of ϕ_c is known. The simulation results for the ϕ_c values for the two cases of cosmological phase transitions and their comparison to the results for equal-size spheres are covered in Section 5. Lastly, in Section 6 we conclude with a discussion of the results and some future prospects for research based on some of the still open questions.

Units

We assume the use of natural units $\hbar = k_B = c = 1$, where c is the speed of light.

2. Cosmological Phase Transitions

At around the electroweak scale temperature $T \approx 100$–1000 GeV the universe undergoes electroweak symmetry breaking, during which the electroweak interaction breaks into the electromagnetic and weak interactions we know today [3]. In addition, the Universe can go through other phase transitions, for example, the QCD phase transition much later in the temperature range of order MeV. We will focus on the phase transition at the EW scale. We briefly discuss cosmological phase transitions in more general context before focusing on the first-order phase transitions, which is the focus of this thesis. The following section closely follows what is discussed in [3–5].

2.1 Electroweak Phase Transition

During the electroweak phase transition, the Higgs field goes from having a zero vacuum expectation value (VEV) $\phi = 0$ to having some nonzero value $\phi \neq 0$. The field in the $\phi \neq 0$ state no longer has the same symmetries as it had before, this process is called spontaneous symmetry breaking and could be a phase transition. Hence, the phase with $\phi = 0$ is often called the *symmetric* phase and the phase with $\phi \neq 0$ *broken* phase or *Higgs* phase. These are also sometimes called the false and true vacuum respectively. The vacuum expectation value of the Higgs field is determined by the minima of the thermal zero-temperature potential $V_0(\phi)$. When the interaction of the field with the other particles is taken into account, the free energy density of the SM particle gas is described by the thermal effective potential $V(\phi, T)$, which is the zero-temperature result with the addition of a contribution from the other particles at finite temperature. During the EW phase transition the present day values for masses of fermions and gauge bosons are set as these depend on the vacuum expectation value. Current knowledge is that for the SM this is a cross-over rather than a true phase transition like that of a first-order which interests us. For the Standard Model, the type of phase transition is determined by the Higgs mass, for masses $m_H \lesssim 75$ GeV the SM phase transition would be of first-order. The present day value of the Higgs mass is around $m_H \approx 125$ GeV [3].

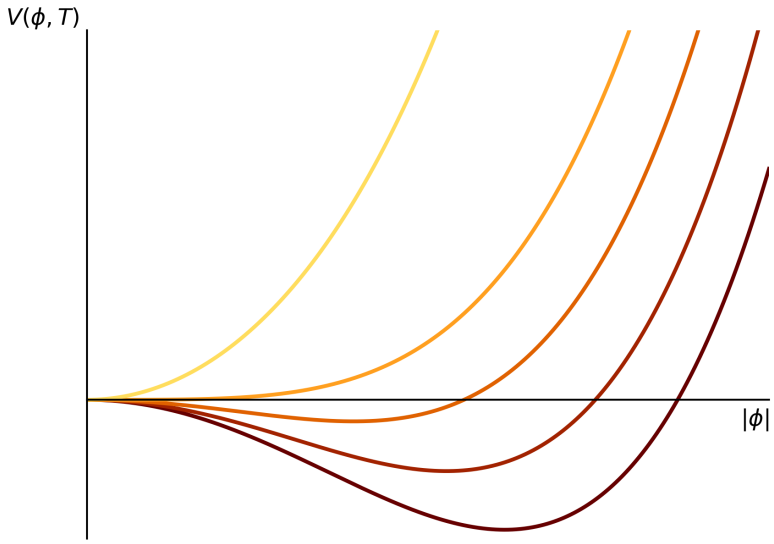

Figure 2.1: Sketch of the first order approximation for the potential of Abelian Higgs field with the SM particles based on [4]. At high temperatures the minima is at $\phi = 0$ but as the temperature drops we develop a new minima at $\phi \neq 0$. In this case the phase transition is not a first-order transition, as the temperature lowers the old minima is smoothly carried away by the lowering of the potential curve and as such there is no discontinuity. Lowering of the temperature is indicated by darkening of the color.

In Figure 2.1 we have a sketch of the thermal effective potential as the Universe cools. At high temperatures we have minima at $\phi = 0$, but as the Universe cools, a new minima develops. In this case, the transition to the new minima respect to the potential value is smooth. This could be a phase transition of second order or a cross-over like in the SM. However, many of the extensions to the SM can under go first-order phase transitions, which are characterized by latent heat, bubble nucleation and a critical temperature, which will be our focus as these have potential to generate gravitational waves which LISA could detect. Since the Standard Model does not undergo a first-order phase transition, the detection of gravitational waves characteristic to one would be an indicator of physics beyond the Standard Model.

First-order phase transitions have an easy real-world example of boiling water which happens through nucleation of bubbles of the new phase and absorption of latent heat. During a first-order phase transition the properties of the system abruptly change, and in the case of water boiling, there is an abrupt change in density. Water freezing also gives an illustrative example of a change in the symmetries of a system during phase transition. Water has translational and rotational symmetry; the system appears on average the same no matter how you continuously translate or rotate it. However, as the water freezes, it forms a crystal structure, and we no longer have

symmetry with respect to an arbitrary rotation or translation [8].

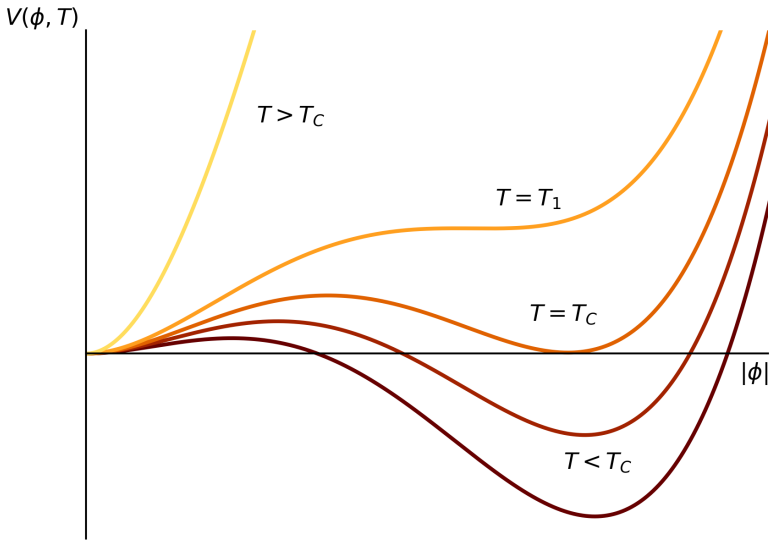

Figure 2.2: Sketch of thermal effective potential for a first-order phase transition based on figure from [3]. At high temperatures $T \gg T_c$ there is a single minima at $\phi = 0$, as the temperature drops at $T = T_1$ a new minima at some $\phi \neq 0$ develops. At $T = T_c$ the new minima is degenerate with the old one and as temperature drops below $T < T_c$ the new minima becomes the global minima. We also see a potential barrier separating the two minima which persists below the critical temperature.

As seen in Fig. 2.2 the minima have a potential barrier separating the two different phases $\phi = 0$ and $\phi \neq 0$. In order to get to the new phase, we must cross this potential barrier. This can happen either via quantum tunneling through it or thermal fluctuations over it. During which bubbles of the new broken phase appear and start growing if they exceed some critical radius R_c and the universe has cooled below the critical temperature T_c. Contrast this with a smooth transition such as a cross-over or a second-order transition as in Fig. 2.1. Additionally, depending on the shape of the potential, we might have that the potential barrier disappears at some temperature such that the completion of the phase transition is guaranteed. We could also have a situation where the Universe never fully transitions to the new phase akin to the graceful exit problem in [7].

2.2 First-order phase transitions

The current research interest lies in the first-order phase transitions, since imprints from such a transition could likely be detectable with the upcoming LISA probe — which is one of its objectives [1, 2]. As the produced spectrum of gravitational waves

is dependent on the phase transition dynamics, we can possibly get new information about physics beyond the Standard Model. From here on out, we will focus solely on the first-order transitions and next discuss some of the relevant quantities during the phase transition. We will later in Sec. 2.3 discuss how the background universe affects these relevant quantities in a strong supercooling case where the transition can be delayed such that the Universe is metastable for an extended duration. In an extreme case the Universe becomes vacuum dominated and can make full transition impossible if the metastability persists down to zero temperature and the expansion of the Universe becomes much greater than the nucleation rate.

In this section, we will give an overview of how the phase transition progresses as the bubbles nucleate and fill the space. We describe the rate at which the bubbles nucleate in Sec. 2.2.1, how the fractional volume in the metastable phase is calculated in Sec. 2.2.2 and finally, we will give an overview of the phenomenon of *percolation* in Sec. 2.2.3, which happens during the phase transition and is one of the milestones for the progress of the transition.

2.2.1 Bubble Nucleation Rate

The first-order phase transition proceeds through nucleation of bubbles of the new phase once we are below the critical temperature T_c. We will now focus our attention on some generalities of the rate at which these bubbles nucleate. The nucleation rate is most often described in physical units of rate per unit volume. The nucleation rate due to thermal fluctuations or quantum tunneling is of the form [9, 10]:

$$\Gamma(T) = A(T)e^{-S(T)} \tag{2.1}$$

where $S(T)$ is related to the solution of a *bounce* action [11], which we will not cover in this thesis. Note that the prefactor also depends on it and is expected to be of the order T_c^4. The solution to the bounce action itself is approximated by either the zero temperature quantum tunneling action $S(T) = S_4(T)$ or the thermal fluctuation action $S(T) = S_3(T)/T$. The zero-temperature quantum tunneling dominates at low temperature, while thermal fluctuation one is dominant at high temperatures [10–12].

As stated earlier, in order for the bubble to grow, the Universe must be cooled below $T = T_c$ and, in addition, the radius of the bubble that forms must exceed a critical radius R_c, which is the radius of a bubble when the forces expanding and shrinking the bubble are balanced. The critical radius depends on the potential difference between the old and new phase $\Delta V_T = V_T(\phi = 0) - V_T(\phi \neq 0)$ [3, 13].

When a bubble first nucleates, the bubble wall accelerates until it reaches a terminal velocity v_w, which is affected by the friction between the bubble wall and the

plasma. The said friction depends on the potential difference ΔV_T [3, 5]. If the friction is not enough to slow down the bubble wall, the wall speed will approach the speed of light $v_w \to 1$. This is expected for a very strongly supercooled phase transition [13, 14]. In a general case, this assumption may not be made if, for example, the friction with the surrounding plasma is significant. However, in certain scenarios we can approximate the bubbles as growing at the speed of light if the effect of the plasma can be neglected for a strong enough transition [13].

As these bubbles grow, they collide and merge to form connected regions where the field is in the broken phase, and eventually if the transition completes the whole universe is in the new Higgs phase as illustrated in Fig. 2.3 below.

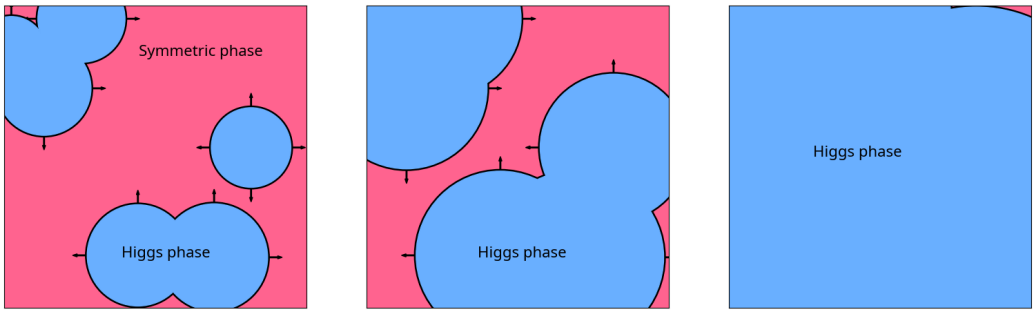

Figure 2.3: Illustration of growth of nucleated bubbles during phase transition. We have bubbles that have nucleated at different times and thus they have different sizes. As the bubbles grow they merge and form connected regions and in certain cases the bubbles of new phase grow such that entire Universe is in the Higgs phase. Illustration based on [3].

A lot of potential energy of the scalar field is released during the phase transition when the field moves to the lower potential state. Part of the energy is transferred to the kinetic energy of the bubbles and heating the plasma [3, 5]. If the bubble grows fast enough as a supersonic detonation, the plasma surrounding the bubble will not be heated, but the interior will be. The three different modes for the bubble wall to expand, these are depicted in Fig. 2.4. If the bubbles grow slowly, the area outside the bubble will be heated, which complicates the transition dynamics and can stop the nucleation of bubbles in the surrounding regions [5]. A proper full treatment of a phase transition requires relativistic hydrodynamics as we need to account for the effect of the plasma. However, we will assume that the heating of the plasma does not play a significant role during the phase transition. Additionally, we assume that the bubbles grow at constant $v_w = c$ speed. In other words, we assume that the bubbles grow as detonations. This is a reasonable approximation for a strongly supercooled phase transition [5], but not necessarily for a fast transition where the friction of the surrounding plasma is expected to play a more significant role.

In the case of strongly supercooled phase transitions where the universe is vacuum dominated, the phase transition can cause the reheating of the Universe and bring it back to radiation domination. This was originally the idea behind the inflation scenario called old inflation now, which ran into the problem where the Universe could get stuck in the metastable phase [7, 15]. Finally, for a fast bubble wall velocity one can approximate the reheating to be instantaneous after percolation [13, 16].

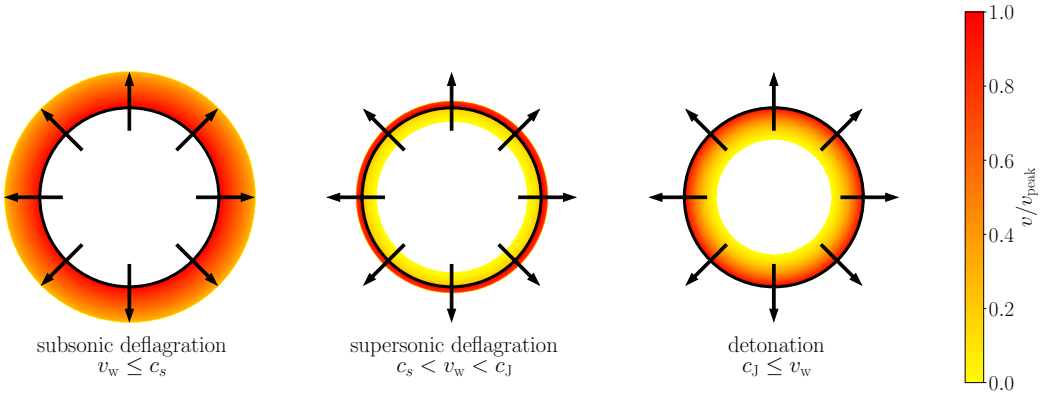

Figure 2.4: Depiction of three modes of bubble expansion, the colored regions depict the speed of the fluid (plasma) around the bubble wall (black). The approximation we use are most applicable to the case where the bubbles expand as detonations, as otherwise the effects of the surrounding plasma are more significant and our approximations no longer work as well. The quantity c_s indicates the speed of sound in the fluid and c_J is Chapman-Jouguet speed. Figure from [3].

2.2.2 Fractional Volume

As the bubbles grow, a larger fraction of the volume will be in the Higgs phase. The fractional volume $h(t)$ still in the symmetric phase can be used to determine the progress of the transition. Note that for a strongly supercooled case with a slow enough nucleation rate, the fractional volume may be misleading as we will see later. In such a case, while $h(t)$ tends to 0, the actual physical volume of the Universe still in the symmetric phase does not decrease due to expansion of the Universe.

As derived in [5], the fractional volume still in the symmetric phase is given by

$$h(t) = \exp(-\mathcal{V}_{\text{ext}}) \tag{2.2}$$

where $\mathcal{V}_{\text{ext}}$ denotes the extended fractional volume the bubbles take up. In other words, in the quantity $\mathcal{V}_{\text{ext}}$ we do not take into account that the bubbles can overlap. The Eq. 2.2 is known as the Johnson-Mehl-Avrami-Kolmogorov (JMAK) equation, which has been known since at least the 1930s [5]. In the context of cosmological phase transition it has also been derived in, for example [17, 18].

The extended fractional volume $\mathcal{V}_{\text{ext}}$ depends on the nucleation rate Γ, bubble

wall speed v_w and the scale factor of the Universe $a(t)$ as [5]:

$$\mathcal{V}_{\text{ext}} = \frac{4\pi}{3}\int_{t_b}^{t}\Gamma(t')a(t')^3R(t',t)^3dt' \tag{2.3}$$

where $R(t',t)$ is the radius of the bubble nucleated at time t' and t_b the time at which nucleation becomes possible.

The JMAK equation 2.2 gives a statistical expression for the fractional volume remaining in the symmetric phase at time t. The JMAK equation relies on some assumptions which are discussed in [5]. We note that it appears some of the assumptions can break down when analyzing cosmological phase transitions, such as the assumption that the bubble nucleation is homogeneous throughout the Universe, which could break for slow bubble walls as discussed briefly earlier. Heuristically speaking, the JMAK equation assumes the existence of phantom bubbles, which are fully contained by the real bubbles. As such, the shape of the bubble and the wall velocity must be such that phantom bubbles cannot outgrow their parent bubbles. In the context of this thesis, none of the assumptions are known to fail, as we assume that the bubbles are spherical and grow with a uniform rate throughout the Universe.

Note the move from temperature to time dependence. Not accounting for a possible reheating, we can use the adiabatic time-temperature relation to write things in terms of temperature [5]:

$$\frac{dT}{dt} = -TH(T) \tag{2.4}$$

where $H(T)$ is the Hubble parameter that can be solved from the Friedmann equation:

$$H^2 = \frac{8\pi G}{3}\rho(T). \tag{2.5}$$

The energy density of the Universe ρ during the phase transition is determined by the configuration of the field. The energy density can be decomposed into different components that scale differently with temperature. Not accounting for a possible subdominant matter contribution, the energy density during the phase transition can be approximated as a part that scales like radiation and vacuum energy [5, 17]:

$$\rho_{tot} \approx \rho_R + \rho_V. \tag{2.6}$$

In the energy density, one could also include the contribution of the bubble walls as is done in [13]. For some strongly supercooled transitions we can approximate the background as vacuum dominated until percolation after which the Universe is reheated and the energy density scales as radiation [13]. If we were to seek an accurate solution, we would have to account for how during the transition the Universe becomes radiation dominated. We would end up with coupled equations since the contribution to the energy density from the phases depends on the fractional volume $h(t)$, which depends on the scale factor, which is itself determined by the total energy density.

2.2.3 Percolation

During the phase transition as the bubbles grow and coalesce to form clusters of bubbles. The system is said to *percolate* when an infinite cluster of bubbles forms. In other words, when we can traverse through arbitrarily large volume via the connected regions made up from the bubbles. We can see a two-dimensional example of this in Figure 2.5 below. Percolation can be used to gauge whether the phase transition completes as this is a necessary, though not sufficient, condition for the volume to be completely filled by bubbles eventually.

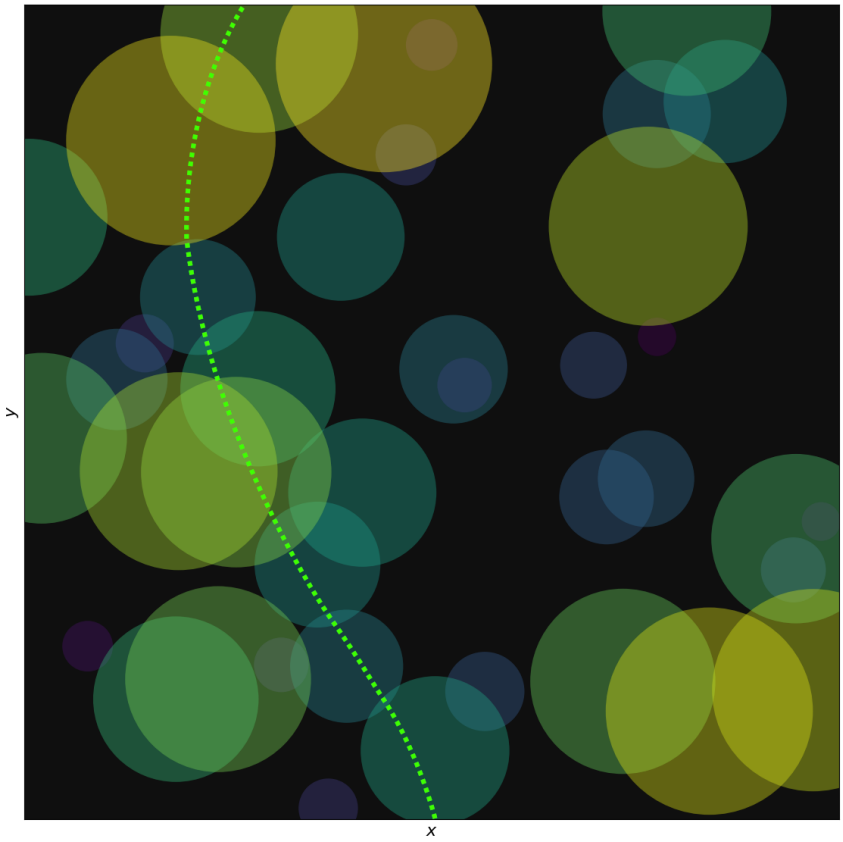

Figure 2.5: A 2D example of percolation of uniformly distributed spheres of different size in a finite volume. The color corresponds to radius of the bubbles. We can find a path across the volume via the bubbles, in this case we could say the system percolates in y direction. In an infinite volume such a distinction in this case is meaningless, however we will return to this later when we simulate the system. Illustration inspired by [14].

The study of percolation is multifaceted with an array of different models and applications. Fundamentally, percolation theory is interested in the formation of connections in a system. As an example, percolation theory can be used to study the coverage of a mobile network, in which case each cell tower would be a *site* and we would study the *bonds* between them. This would be called bond percolation, as op-

posed to site percolation, where the sites directly adjacent to one another are either occupied or unoccupied. Another classification is whether one studies percolation in a lattice versus a continuous media. The former falls under discrete percolation theory and the latter under continuum percolation theory. For a general introduction to percolation theory, see [19, 20] with continuum percolation discussed in detail in [21]. Bubble nucleation would fall under continuum percolation, but one could likely also use a lattice to study it.

Usually percolation is a critical phenomenon such that below a certain threshold there never exists a system spanning cluster, and above the threshold one always exists. Percolation can be studied in a finite system, but our focus will lie on an infinite system, where the percolating cluster is also infinite. Note that there are potentially infinite number of systems that can be made from, for example graphs, the features identified in one system may not necessarily apply to others. As an example, if the d-th moment of the radius distribution r is infinite, then no critical threshold for percolation exists [22].

The case of cosmological phase transitions we describe in this thesis is similar to the Boolean model as described in [21, 23]. In the Boolean model it has been proven that a critical value for percolation exists [21]. However, the growth of bubbles as we described probably falls outside the realm of Boolean model. The Boolean model assumes that the placed spheres are driven by stationary point process among other things. In our case, the process is not likely stationary, since when we look at our system, the distribution of radii is not translationally invariant. We have a clear time dependence on bubble sizes which is reflected spatially because bubbles are not able to nucleate inside already nucleated bubbles. However, the difference is subtle, as only certain configurations where the bubble has nucleated inside another bubble and covers area outside the parent bubble are forbidden. We allow the occurrence of phantom bubbles that are fully covered by another bubble, which brings the process closer to being stationary. As such, it is not clear how significant breaking the stationary assumption is in this case, which should be studied further.

There are likely other subtle nuances that are outside the scope of this thesis. We will assume that when percolation can occur, there exists a critical fractional volume $\phi_c = 1 - h_c$ taken up by the bubbles such that for $\phi < \phi_c$, percolation does not occur, and for $\phi > \phi_c$, it always occurs. One of the goals of this thesis is to determine the critical value for two cases, which we will discuss in Section 2.3, and whether they differ significantly from the result for the Boolean model. We will note t_p as the time during the phase transition when percolation occurs, in other terms $\phi_c \equiv \phi(t = t_p) = 1 - h(t = t_p)$.

To our knowledge, no one has found the result for ϕ_c in the context of cosmological

phase transitions, instead the Boolean model result of uniformly distributed equal-sized spheres $\phi_c \approx 0.288 - 0.290$ has been used in numerous cosmology papers [5, 13, 16, 17]. This is expected to approximate the critical value for in cosmological phase transition. We will not necessarily find out if this is the case for all possible transitions, as we should expect the transition dynamics to play a role in determining the value of ϕ_c. For example, in [24] it was found that for a mixture of spheres of two different sizes, the percolation threshold ϕ_c varies depending on the ratio of the sphere radii. As such, we should draw the conclusion that there may not be a single ϕ_c value that is applicable for all cases.

Although there may be no universal ϕ_c value, there may be some universal properties of the system. From studies of other percolating systems, it has been found that there are power laws that describe the behavior of the system near criticality very well and have been found to be universal so far [20]. Some interesting quantities that follow such power laws are for example the probability P that a cluster belongs to the infinite cluster and the correlation length ξ, which gives the size of typical cluster or the scale at which the system is homogeneous, for these power laws near p_c are given by [19, 20]:

$$P \propto (p - p_c)^{\beta} \tag{2.7}$$

$$\xi \propto (p - p_c)^{-\nu} \tag{2.8}$$

where case p is the probability that a certain site/bond is connected. This comes from the discrete percolation theory, but these results can also be assumed to work for continuum percolation [20]. In our case, we can assume that the probability that we have percolation is related to the fractional volume $\phi = 1 - h$.

Interesting to note is that the correlation length might help predict whether or not primordial black holes can be produced during the phase transition. It has been suggested that primordial black holes might be produced in regions where the symmetric phase is still surrounded by regions in the broken phase [25], since the correlation length can also give the typical size of an empty region [20].

An important scaling law for this thesis, which has been used in several sources* is [26–29]:

$$\phi_c(L) - \phi_c \propto L^{-1/\nu} \tag{2.9}$$

where $\phi_c(L)$ is the critical value for percolation of finite subvolume of L^3 that we obtain from a function that approaches a step function such as [26]:

$$\frac{1}{2}\left(1 + \operatorname{erf}\left(\frac{\phi - \phi_c(L)}{\Delta(L)}\right)\right) \tag{2.10}$$

*We believe the same might be found in [19] with more rigorous detail, but we could not confirm it.

where $\Delta(L)$ is the width of the transition, which scales as

$$\Delta(L) \propto L^{-1/\nu}. \tag{2.11}$$

These exponents of the scaling laws are called *critical exponents* and are universal and depend only on the Euclidean dimensionality [19, 20]. We will assume that our systems follow this scaling, but we will later see that this scaling gives a result for the equal-sized sphere case in agreement with $\phi_c \approx 0.288 - 0.29$ with decent accuracy. However, the data indicates that the critical exponent in the scaling of Eq. (2.9) is different from the known value of $\nu \approx 0.88$ [19, 20] if we do not have any systematic error in our analysis or simulation. This could also be due to the finite-size scaling law having a different form for the exponent–or the resolution of our data is simply not high enough. We should also note that in [29] the critical exponent was consistently larger than expected for cuboid particles, but this might also be due to the exponent of the scaling law for ϕ not being solely dependent on ν as we suggest.

2.2.4 Transition Milestones

We will now look at some relevant milestones during the phase transitions. Each of these are in terms of time t_i, but there exists a corresponding temperature T_i. Note that reheating can complicate the relation between time and temperature, but this can be ignored as an approximation in strongly supercooled transitions [14]. As such, it is heuristically easier to talk of them in terms of physical time.

Time of critical temperature t_c

The time when the temperature drops below the critical temperature $T_c(t_c)$ for the first time and the transition becomes possible.

Time of reheating t_{reh}

The time when the transition has completed and that the Universe is reheated up to the temperature T_{reh}, which can be obtained as an approximation from the percolation temperature T_p [5].

Unit Nucleation Time t_n

The unit nucleation time t_n is defined as the time when one bubble per Hubble volume has nucleated on average, also referred to as unit nucleation. This often is thought to mark the time when the phase transition starts, as at $T = T_c(t = t_c)$ there is no significant nucleation. However, as argued in [14], percolation can happen without unit

nucleation and vice versa. As such, the nucleation time is not a significant milestone during some phase transition, but it can be used to predict GWs from a fast transitions as the relevant milestones happen in a shorter window of time.

Peak Nucleation Time t_f

Another used milestone is the time $h(t_f) = 1/e$, which we use in the case of a fast transition. In the case of the fast transition discussed later, the time t_f coincides with the maximal rate of change of the fractional volume, in other terms $\ddot{h}(t_f) = 0$ and $\dot{h}(t_f) > 0$ [3]. One could also find t_e for the slow transition discussed later, but for certain cases $\ddot{h}(t) = 0$ does not exist during the phase transition.

Percolation time t_p

The percolation time t_p is defined as the time when percolation occurs, this can be calculated from the condition $\phi_c = 1 - h_c(t_p)$, where ϕ_c was the critical fractional volume of bubbles for percolation to occur as described in Sec. 2.2.3. The percolation time t_p is often used to approximate the time when GWs are produced in a strongly supercooled transition [11, 13, 16]. Realistically, the GW production happens throughout the phase transition, so in the cases of a slower transition there might not be a single good reference time for this [5]. Note that the energy stored in the bubble wall is proportional to the radius of the bubble and the potential difference across it, which in turn plays a role in the contribution of collisions to the GW signal [13].

Completion time t_v

For a complete phase transition we would expect that eventually the Universe is in one phase such that $h(t_v) = 0$. As mentioned earlier, $h(t)$ may asymptotically vanish when looking at the comoving volume, even though the transition may not complete. Sometimes also some small threshold is used such that the completion time is taken to be when $h(t_v) = \epsilon \ll 1$ [5].

2.3 Case of a Slow and a Fast Transition

We will now focus on the case of a fast transition, as discussed in [3, 12, 14] and a slow transition similar to [7]. We now focus on what happens after the bubbles have nucleated and how the system evolves in both cases. In the case of a fast transition, the nucleation rate is dominated by the finite temperature $S_3(T)$ bounce action. In addition, we assume that the transition is fast enough that we can neglect the expansion

of the universe. For the slow transition, we assume that it is driven by a constant zero-temperature quantum tunneling rate Γ_0 as described in [7]. This would be the case if the universe remained metastable down to zero-temperature, one would also expect this transition to produce more violent GWs. An additional motivation for studying the case is that the constant nucleation rate is simple to handle. However, we should note that in general a slow transition could possibly happen at a finite temperature when the nucleation rate compared to the Hubble rate is small $\Gamma_0/H^4 \ll 1$.

As stated earlier, we assume that the bubbles are spherical, grow at the same rate uniformly in all directions, and after colliding with each other, they continue to grow with the same rate while remaining spherical. We also assume that the initial size of the bubble is negligible. We should add that, for a more realistic case, one should probably have to take into account how the expansion rate inside the bubbles affects the dynamics, in addition to accounting for what happens at the boundary of the bubbles where the expansion rate differs inside and outside the bubble. However, with strong enough supercooling, one can approximate the Universe as being vacuum dominated until percolation [13].

2.3.1 Fast transition

We will now describe a fast transition with an exponential nucleation rate. As stated, for a fast transition, we assume that the transition happens fast enough such that we can neglect the expansion of the Universe. In such a case, we can take the nucleation rate to be given by Taylor expansion of $\log\Gamma$ by defining a transition rate parameter as follows [3]:

$$\beta = \frac{d}{dt}\log(\Gamma(t))\Big|_{t=t_f} \tag{2.12}$$

where t_f is defined as $h(t_f) = 1/e$. To a first-order Taylor expansion this gives

$$\Gamma(t) = \Gamma_f e^{\beta(t-t_f)} \tag{2.13}$$

and Γ_f is given by

$$8\pi\frac{v_w^3}{\beta^4}\Gamma_f = 1. \tag{2.14}$$

We can approximate the bubbles to grow at the speed of light, as v_w together with β gives the physical units of length and as such it is a matter of scaling the quantities if we were to choose another v_w [12]. Of course, we also must assume that we do not have significant interactions between the bubble walls and the plasma surrounding it such that the nucleation rate remains homogeneous throughout the false vacuum.

For $v_w = c = 1$, the bubbles grow as

$$R(t', t) = t - t' \tag{2.15}$$

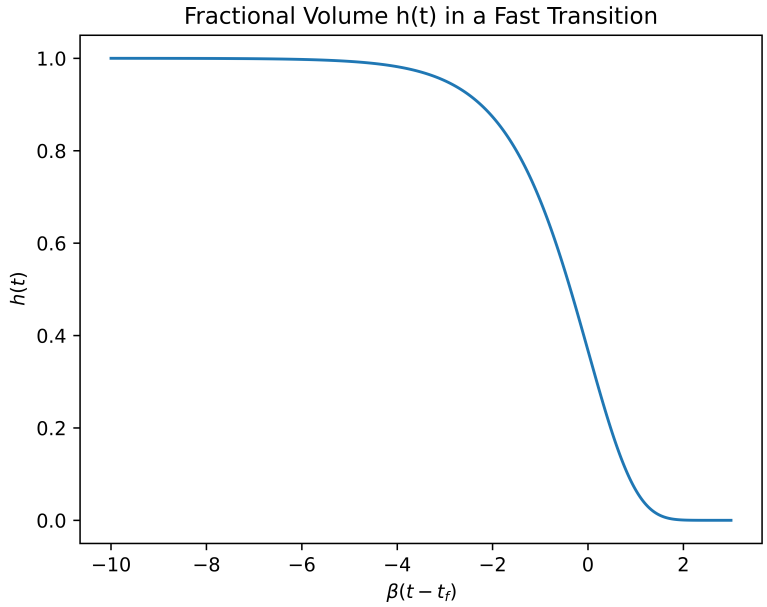

Figure 2.6: Plot of the fractional volume $h(t)$ in a fast transition as given by Eq. (2.16) as function of $\beta(t - t_f)$.

where t' is the time the bubble nucleated. Now the transition always completes, as under the assumptions we use nothing is impeding the expansion of the bubbles. Now, using Eq. (2.2) we get the fractional volume remaining in the metastable phase by performing a saddle-point approximation [3]:

$$h(t) = \exp\Big(-e^{\beta(t-t_f)}\Big). \tag{2.16}$$

Plotting this as a function of $\beta(t - t_f)$ gives us Figure 2.6, and as noted earlier, $t = t_f$ coincides with the peak rate of change for the fractional volume $h(t)$.

The mean number of bubbles in a given volume V is given by [3, 12]:

$$N(t) = \frac{\Gamma_f V}{\beta}(1 - h(t)). \tag{2.17}$$

From this we can also see that the final mean number of bubbles approaches the value given by $N_f \equiv N(t \to \infty) = \Gamma_f V/\beta$. Additionally, the final mean density of bubbles $n_f = \Gamma_f/\beta$ defines the mean separation of bubble centers $R_* = (n_f)^{-1/3}$ [3].

We can also calculate the distribution of the bubble radii from Eq. (2.17) in the following manner. The mean number of bubbles at time $t = t'$ when a bubble nucleates is given by Eq. (2.17) as $N(t')$. Using Eq. (2.15) we get the mean number of bubbles at time t that are smaller than r:

$$N(r, t) = N_f(1 - \exp\Big(-e^{\beta(t-r-t_f)}\Big)). \tag{2.18}$$

Taking a differential respect to time t gives us the mean number density, or the distribution of bubbles of radii r as seen at time t in the volume V. We also need to take into account that bubbles have a maximum size of $r_m(t) = t - t_b$, where t_b is the time when the first bubble nucleates. As such, we have to include a cutoff $\theta(r_m(t) - r)$ with the Heaviside function:

$$\frac{dN(r,t)}{dt} = \Gamma_f V \exp\Big(-e^{\beta(t-r-t_f)}\Big) e^{\beta(t-r-t_f)}. \tag{2.19}$$

The distribution of bubble radii does not, at least on the surface, tell much about the percolation threshold $\phi_c = 1 - h_c$. Nonetheless, we would argue that it does provide a slight indication as to whether or not we should expect the percolation threshold to change. As was found in [24], for two different sized spheres the threshold changed based on the ratio of the bubble radii, which would indicate that the distribution of bubble radii may have an effect on the threshold ϕ_c. The physical units of time are given by $t_{growth} = 1/\beta$, in this case if we scale our units with respect to β the distribution looks the same for all β.

2.3.2 Slow transition

We will follow the assumptions made in [7] where we have very strong supercooling such that the Universe has cooled enough that the expansion is dominated by vacuum energy. We assume that bubble nucleation is driven by zero-temperature quantum tunneling, which is the case when the thermal production of bubbles becomes subdominant at low temperatures [7]. We assume that the potential barrier between the phases exists down to zero temperature, but this is not necessarily a general feature of strong supercooling. Finally, we assume that the bubbles grow at speed of light such that the regions outside the bubbles are not affected by the growth of the bubbles.

We assume that the metric of the Universe is given by the flat FLRW metric.

$$ds^2 = -dt^2 + a(t)^2(dr^2 + r^2 d\Omega^2) \tag{2.20}$$

where $d\Omega^2 = d\theta^2 + \sin\theta d\varphi$ is the usual angular part of the metric. If the vacuum energy dominates, the scale factor is given by $a(t) = e^{Ht}$. We choose $a(t = 0) = 1$ to be at the start of bubble nucleation t_b and $H = H(t = 0)$. We can perform a change of variables to conformal time $d\eta = dt/a(t)$:

$$ds^2 = a(\eta)^2(-d\eta^2 + dr^2 + r^2 d\Omega^2) \tag{2.21}$$

Further, calculating the relation between conformal time and physical time yields

$$\int d\eta = \int e^{-Ht} dt \implies \eta = -\frac{1}{H} e^{-Ht} + C. \tag{2.22}$$

Now we choose to set $\eta = 0$ to correspond to $t \to \infty$ so that the integration constant is zero. The scale factor $a(t) = 0$ now corresponds to $t \to -\infty$, and $t = 0$ in the new coordinates is mapped to $\eta \to -\infty$. As such, the conformal time coordinate has a range of $\eta \in (-\infty, 0]$. From the form of Eq. (2.22) we immediately see what the scale factor in terms of conformal time is given by

$$a(\eta) = -\frac{1}{H\eta}. \tag{2.23}$$

Using conformal time and comoving coordinates, the radius of the bubble is given similar to Eq. (2.15):

$$R(\eta', \eta) = \eta - \eta' \tag{2.24}$$

where η' is the conformal time the bubble nucleated. The bubbles will asymptotically grow to a finite size given by

$$R_{asym} = R(\eta', 0) = -\eta' = \frac{1}{H} e^{-Ht'}. \tag{2.25}$$

Since we assume a constant nucleation rate Γ_0, the fractional volume given by the JMAK equation Eq. (2.2) in this case is

$$h(t) = \exp\left(-\frac{4\pi}{3}\int_{t_b}^{t} \Gamma_0 a(t')^3 R(t', t)^3 dt'\right) \tag{2.26}$$

changing to conformal time with $d\eta = dt/a(t)$ and using Eq. (2.23) gives us

$$= \exp\left(-\frac{4\pi}{3}\int_{\eta_b}^{\eta} \Gamma_0 \frac{1}{H^4\eta'^4}(\eta - \eta')^3 d\eta'\right). \tag{2.27}$$

While a slightly tedious calculation, it is analytically trivial to calculate and is done in the appendix A.7 giving us:

$$h(\eta) = \exp\left(-\frac{4\pi}{3}\frac{\Gamma_0}{H^4}\left[\frac{1}{3}(\frac{\eta}{\eta_b})^3 - \frac{3}{2}(\frac{\eta}{\eta_b})^2 + 3\frac{\eta}{\eta_b} - \ln\left(\frac{\eta}{\eta_b}\right) - \frac{11}{6}\right]\right). \tag{2.28}$$

Note that as $\eta \to 0$ the logarithm diverges $\ln(\eta/\eta_b) \to -\infty$ such that $h(\eta) \to 0$. However, percolation in this case is still questionable [7]. Instead, a better metric is the physical volume of the false vacuum $V_{false} \propto a(t)^3 h(t)$ and its change, which should become negative after time $\eta_e \propto t_e$ where $t_e \lesssim t_p$. This gives us a condition for the occurance of percolation [30]:

$$\frac{1}{V_{false}}\frac{dV_{false}}{dt} = \frac{1}{a(\eta)V_{false}}\frac{dV_{false}}{d\eta} < 0. \tag{2.29}$$

For the slow transition the condition is given by

$$\frac{1}{a(\eta)a^3(\eta)h(\eta)}(3a'(\eta)a(\eta)^2h(\eta)+\frac{dh(\eta)}{d\eta}a^3(\eta))<0 \tag{2.30}$$

$$\frac{1}{a^4(\eta)h(\eta)}\left(3a'(\eta)a(\eta)^2h(\eta)+(-\frac{4\pi}{3}\frac{\Gamma_0}{H^4}\left[\frac{\eta^2}{\eta_b^3}-3\frac{\eta}{\eta_b^2}+\frac{3}{\eta_b}-\frac{1}{\eta}\right])h(\eta)a^3(\eta)\right)<0 \tag{2.31}$$

$$3H+(-\frac{1}{a(\eta)}\frac{4\pi}{3}\frac{\Gamma_0}{H^4}\left[\frac{\eta^2}{\eta_b^3}-3\frac{\eta}{\eta_b^2}+\frac{3}{\eta_b}-\frac{1}{\eta}\right])<0 \tag{2.32}$$

$$3+\frac{4\pi}{3}\frac{\Gamma_0}{H^4}\left[\frac{\eta^3}{\eta_b^3}-3\frac{\eta^2}{\eta_b^2}+\frac{3}{\eta_b}\eta-1\right]<0 \tag{2.33}$$

where we have used the fact that $H=a'(\eta)/a(\eta)^2$ at Eq. (2.32). This can be regarded as one of the necessary conditions for a complete transition, and percolation can be considered questionable if this condition is not met during the time $t_p(\eta_p)$ percolation should occur. Based on this, we can get a minimal condition for percolation when we require that the condition Eq. (2.33) is satisfied before $\eta=0$:

$$\frac{\Gamma_0}{H^4}>\frac{9}{4\pi}. \tag{2.34}$$

Next, we take the derivative of $h(\eta)$ and examine its behavior when $\eta\to 0_-$, or in other terms $\eta/\eta_b\to 0_+$ as $\eta,\eta_b<0$. Using the limit of a product rule, we get

$$\lim_{\eta\to 0_-}\left(-\frac{4\pi}{3}\frac{\Gamma_0}{H^4}\left[\frac{\eta^2}{\eta_b^3}-3\frac{\eta}{\eta_b^2}+\frac{3}{\eta_b}-\frac{\eta_b}{\eta}\right]h(\eta)\right)=\lim_{\eta\to 0_-}\left(\frac{4\pi}{3}\frac{\Gamma_0}{H^4}\left[\frac{\eta_b}{\eta}\right]h(\eta)\right) \tag{2.35}$$

Now substituting in $h(\eta)$ from Eq. (2.28) gives

$$=\lim_{\eta\to 0_-}\left(\frac{4\pi}{3}\frac{\Gamma_0}{H^4}\left[\frac{\eta_b}{\eta}\right]\exp\Big(-\frac{4\pi}{3}\Gamma_0\frac{1}{H^4}\left[\frac{1}{3}(\frac{\eta}{\eta_b})^3-\frac{3}{2}(\frac{\eta}{\eta_b})^2+3\frac{\eta}{\eta_b}-\ln\Big(\frac{\eta}{\eta_b}\Big)-\frac{11}{6}\right]\Big)\right) \tag{2.36}$$

$$=\lim_{\eta\to 0_-}\left(\frac{4\pi}{3}\frac{\Gamma_0}{H^4}\left[\frac{\eta}{\eta_b}\right]^{\frac{4\pi}{3}\frac{\Gamma_0}{H^4}-1}\exp\Big(-\frac{4\pi}{3}\Gamma_0\frac{1}{H^4}\left[\frac{1}{3}(\frac{\eta}{\eta_b})^3-\frac{3}{2}(\frac{\eta}{\eta_b})^2+3\frac{\eta}{\eta_b}-\frac{11}{6}\right]\Big)\right). \tag{2.37}$$

From this we can see that the limit is zero if

$$\frac{4\pi}{3}\frac{\Gamma_0}{H^4}-1>0. \tag{2.38}$$

This indicates that there is possibly some change in behavior around $\Gamma_0/H^4\sim 3/4\pi$ at which the limit tends to a constant value of

$$\lim_{\eta\to 0_-}\frac{dh(\eta)}{d\eta}=\frac{4\pi}{3}\frac{\Gamma_0}{H^4}\exp\left(\frac{4\pi}{3}\frac{\Gamma_0}{H^4}\frac{11}{6}\right). \tag{2.39}$$

For values smaller than this, the limit goes as $\lim_{x\to 0_+}e^{-x}/x^a$, where $-1\le a<0$ as $\Gamma_0/H^4>0$ for physical reasons. In such a case, we have a positive divergence. Note the use of the one-sided limit as $\eta<0$, since where the limit diverges the double-sided

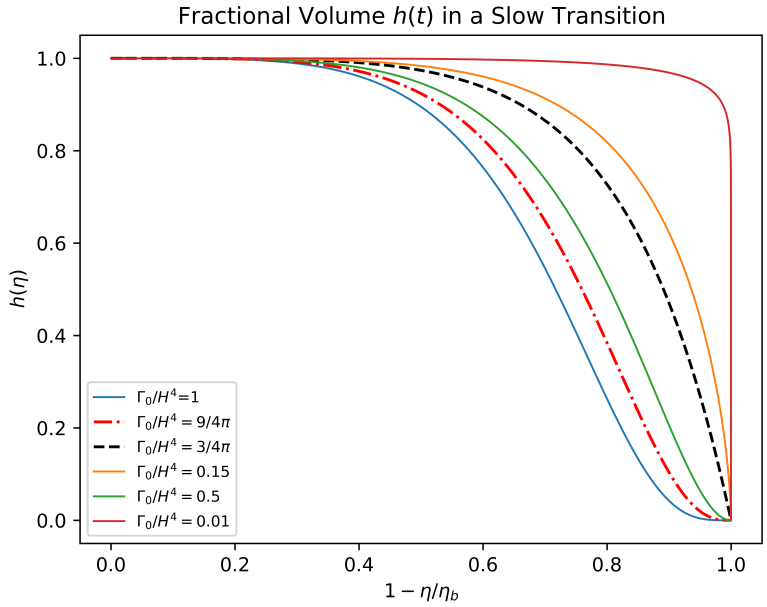

Figure 2.7: Plot of Eq. (2.28) for different Γ_0/H^4 values. The black dashed line is the value after which the derivative at $h'(\eta \to 0)$ starts to diverge coming from Eq. (2.38). The red dot dashed line is the condition Eq. (2.34). Note that behavior for value of $\Gamma_0/H^4 = 0.01$ where the $h(\eta)$ very sharply goes to 0 as $\eta \to 0$ despite percolation being questionable at this point. The plot of $h(\eta)$ for large enough Γ_0/H^4 is similar to that of Fig. 2.6.

limit does not exist. In Figure 2.7 we can see how the behavior changes with different values of Γ_0/H^4.

The mean number of bubbles in a given comoving volume is given by

$$N(\eta) = \int_{\eta_b}^{\eta} \Gamma_0 h(\eta') a^4(\eta') V d\eta' \tag{2.40}$$

where η' is an integration variable. This integral is complicated and might not have a closed-form expression. However, it is numerically solvable for $\eta \neq 0$. Despite this, we can acquire the distribution of bubble radii analytically in the same manner as before. Consider now η' the time when a bubble nucleates, not to be confused with the integration variable above. Using $r = \eta - \eta'$ we get the mean number of bubbles at time η that are smaller than r as

$$N(\eta, r) = \int_{\eta_b}^{\eta - r} \Gamma_0 h(\eta') a^4(\eta') V d\eta'. \tag{2.41}$$

Using the Leibniz rule, we can differentiate with respect to conformal time η to obtain the mean number density as a function of the radius r at time t.

$$\frac{dN(\eta, r)}{d\eta} = \Gamma_0 h(\eta - r) a^4(\eta - r) V \frac{d}{d\eta}(\eta - r) = \frac{\Gamma_0}{H^4 (\eta - r)^4} V h(\eta - r) \theta(r_m - r)$$

where we have included the cutoff for the maximum size of a bubble $r_m = \eta - \eta_b$ in the last step. We can compare this result to that in [7] and see that this gives the same result if we assume the existence of phantom bubbles by setting $h(\eta - r) = 1$. We can see that Γ_0/H^4 fixes the shape of the distribution.

2.4 Gravitational Waves from first-order PTs

As described by the theory of general relativity, gravitational waves are perturbations in spacetime that travel at the speed of light. We will not go into detail on the topic, as it is covered well elsewhere, for example in [31]. In general, gravitational waves are generated from an asymmetric distribution of accelerating masses, for example merging of massive binary astrophysical objects like black holes. Specifically, when the quadrupole moment of the system is nonzero. For example, a spherically symmetric distribution of masses will have zero quadrupole moment and will not source any GWs even if the masses were accelerating [3, 4]. In addition to astrophysical sources, gravitational waves can also be generated by cosmological sources like first-order PTs as discussed or quantum fluctuations during inflation [1].

The effect of gravitational waves on matter can be described as stretching and compressing spacetime in a plane perpendicular to the direction of propagation [3, 31]. The effect from sources at astronomical scales relevant to us is microscopi and very difficult to detect. Detecting them was accomplished in 2015 by the Laser Interferometer Gravitational-Wave Observatory (LIGO) after it detected the merging of two black holes [32]. The basic operating mechanism of LIGO is to measure this minute stretching and compression of spacetime by splitting and bouncing a laser beam along two equally long paths perpendicular to each other. If either path was stretched or compressed, there will be an interference pattern when the light beams are combined. The Laser Interferometer Space Antenna (LISA) will operate in a manner similar to LIGO. LISA consists of three satellites orbiting the Earth that can measure the time delays of laser signals sent between the satellites [3]. The resulting signal from a first-order transition is likely to be in the range detectable by LISA [1, 3, 16].

The generation of GWs from a first-order transition is an involved process, and the prediction of the resulting spectrum of GWs from a specific particle physics model often requires a lot of numerical methods. We will briefly discuss some of the generalities in regard to which events during a first-order PT source GWs. Gravitational waves generated from a first-order phase transitions would contribute to the stochastic gravitational wave background. The stochastic background is isotropic akin to the Cosmic Microwave Background and is characterized by the power spectrum $\Omega_{GW}(f)$. Signals from foreground astrophysical events would in contrast be anisotropic, apart from an

unlikely scenario where there are several astrophysical events of the same type for a long period of time [5].

There are three main ways gravitational waves can be generated during a first-order phase transition [3–5]:

1. From the collisions of bubble walls. Initially the bubbles are spherically symmetric and as such will not source GWs, however this symmetry is broken when the bubbles collide. This is expected to be subdominant unless the friction due to the plasma surrounding the bubbles can be neglected, in which case the bubble walls runaway and become a dominant source of GWs during the phase transition.

2. The collisions of the bubble walls leave propagating imprints on the fluid plasma as *sound waves*. As the fluid kinetic energy in the plasma propagates, it overlaps and collides with sound waves sourced from collisions elsewhere. As these waves overlap they can produce gravitational waves. The sound waves are expected to be the dominant contribution to the GW spectrum unless the transition is very strong or the bubble size is in the same order as the cosmological horizon.

3. Turbulent phase, where the non-linear nature of the fluid equations becomes relevant, during which the fluid might develop vorticity, turbulence or shocks.

The total contribution of each source to the power spectrum Ω can be approximated as a sum of the power spectra from the different sources. Contribution of each source to the resulting GW spectrum depends on the transition dynamics. Some of the key quantities in predicting the resulting GWs are the efficiency of vacuum energy conversion into other forms like the kinetic energy of the bubble wall, the transition temperature, the bubble wall speed v_w, the transition strength α, and the characteristic time scale of the transition [3, 5]. In the case of a fast transition, for example, the characteristic time is given by $1/\beta$. For the transition temperature either the nucleation temperature T_n, the percolation temperature T_p, the completion temperature T_v or the reheating temperature T_r is used in the literature [3, 5, 16].

3. Simulation Methods

In this section, we will develop simulation methods for bubble nucleation and detection of percolation. We make the simplifying assumption that the bubble shape is spherical and that the nucleation rate is homogeneous in false vacuum which, as stated earlier, might not always be applicable. Additionally, we neglect the initial size of the bubbles, as the initial sizes are very small, which is also an assumption of the JMAK equation [5]. We also use periodic boundary conditions (PBC) to approximate an infinite volume in the simulation. From the data, we will calculate the critical fractional volume ϕ_c at which percolation occurs during the phase transition. The basic framework for simulating bubble nucleation is as described in [12]. In addition to this, we also need a couple of methods for finding all the clusters of connected bubbles and checking whether a certain cluster is the percolating cluster. We will also discuss the relevant optimization methods that are applied to each component of the simulation.

3.1 Preliminaries

Firstly, since we do not want to check every bubble against every other bubble, we divide the volume into cubic cells of size $2r_{max}$ where r_{max} is the radius of the largest bubble possible during the simulation, which is given by Eq. (2.15) or Eq. (2.24). The cell coordinates $\vec{a}$ can be calculated from the center of the bubble coordinates as

$$\vec{a}_{cell} = \left\lfloor \frac{\vec{a}}{2r_{max}} \right\rfloor \tag{3.1}$$

where $\vec{a} = (a_1, a_2, a_3)$ is the location of the center of the bubble and $\lfloor\ \rfloor$ the floor function. With this we can limit the number of bubble comparisons to just the neighboring cells. So, at this stage one should already know what data structure to use so we can identify the cell to which each bubble belongs. Note that we also need to add an exception for boundary cells such that the search wraps around to the cell on the other side. This is utilized in Section 3.2 when checking whether the location is within a bubble, but not with cluster finding. An important note is that there was an oversight in the actual implementation and the cell search wrapping around the volume was left

out in the nucleation algorithm. This should not have a major impact on the results, as we expect this to be an edge effect, which makes the simulation of smaller volumes less accurate.

At this stage we should mention that in addition to knowing which cell the bubbles belong to, the bubbles should also have couple boolean values which we will describe later during the cluster finding. In addition, the bubbles have some coordinates and a radius.

We also have to consider how the distances are calculated with the periodic boundary conditions. If the distance between points along any direction is greater than half of the boundary, then wrapping around the volume along that direction is the shorter path. We calculate the shortest distance between two points $\vec{x}, \vec{y}$ as follows: given a boundary size L, such that for all coordinates a_i we have $a_i \in [0, L]$, then the shortest distance between the points is given by

Algorithm 1 An algorithm for calculating the shortest distance in PBC.

```
Δv ← |x⃗ − y⃗|
if Δv_i > L/2 then
    Δv_i ← L − Δv_i
end if
```

There are likely methods to further optimize the simulation to be even faster. As one suggestion, we should be able to further optimize the simulation by placing some of the largest bubbles into a separate data structure, allowing the cell size to be shrunk. This has not been done in this thesis, as its impact might not be significant enough to warrant it.

3.2 Nucleation of bubbles

The following simulation, as outlined in [12] is based on the Poisson process. The assumption that the nucleation can be modeled as a Poisson process underlies the assumptions in the JMAK equation [5]. As such, for a Poisson process the probability of no bubbles nucleating between times t_1, t_2 is given by [12, 33]:

$$p(t_1, t_2) = \exp\Big(-\int_{t_1}^{t_2} V\Gamma(t)dt\Big) \tag{3.2}$$

For fast transitions with nucleation rate Eq. (2.13) we can perform a change of variables to more convenient time coordinate $\tau = \beta(t - t_f)$, as is done in [12], yielding

$$p(\tau_1, \tau_2) = \exp\left(-\int_{\tau_1}^{\tau_2} \frac{V\Gamma_f}{\beta} e^{\tau} dt\tau\right) \tag{3.3}$$

Note that the constant factor is the final mean number of bubbles in the given volume $N_f = \Gamma_f V/\beta$.

We now start from an initial time $t_1 = \tau_1 = -\infty$ and we want to generate a random number $r \in [0, 1)$ and solve the next nucleation time* from

$$p(\tau_1, \tau_2) = r \implies \tau_2 = \ln\left(e^{\tau_1} + \frac{\Gamma_f V}{\beta} \ln\left(\frac{1}{r}\right)\right). \tag{3.4}$$

When we start from $\tau_1 = -\infty$, τ_2 is the time when the first bubble nucleates. As such, we need to add this bubble to our volume, change $\tau_2 = \tau_1$, then go back to generating a new τ_2 and continue as we will describe next.

Now we increase the radius of all the bubbles by the amount they have grown during the time $\tau_2 - \tau_1$, which in this case is given by $\beta^{-1}(\tau_2 - \tau_1)$. Afterwards, we choose a random location within the volume and check whether it is inside a bubble or not. If the location is not inside a bubble, we place a new bubble there, otherwise we reject the bubble. Finally, we replace τ_1 with τ_2 and return to generating a random number and finding the next nucleation time. This continues until we reach some desired final time τ_f.

To summarize, the steps are as follows:

1. Begin at time $\tau_1 = -\infty$ and solve the first nucleation time from Eq. (3.4) and place the bubble in a random location and set $\tau_2 = \tau_1$.

2. Solve τ_2 from Eq. (3.4).

3. Loop through all the bubbles and grow them by amount $\Delta r = \frac{1}{\beta}(\tau_2 - \tau_1)$

4. Check if random location is inside a bubble or not, if it isn't place a new bubble there, otherwise skip adding bubble.

5. Set $\tau_2 = \tau_1$ and loop back to Step 2 until we reach the chosen final time τ_f, which ends the simulation.

Note that Steps 3 and 4 are performed in the opposite order to [12], which we believe might introduce a slight error, as a bubble may be placed inside another bubble if the check is performed before growing the bubbles. The effect of this should be small in most cases. During this process, we also place the bubbles into the cells. In Step 4, we already use the cells such that only neighboring cells are checked, which significantly speeds up the simulation with a large number of bubbles. One should use the cell search that wraps around the volume here.

*Note the typo in [12] Equation 4.14, as it should read $\ln(1/r)$ instead of $\ln(1/4)$.

For the parameters, we can fix $\Gamma_f = 1$ and set the wall velocity to $v_w = 1$ as the physical units of time are given by $t_{growth} = 1/\beta$ and the length by $v_w t_{growth}$ [12]. Thus, changing $\Gamma_f = 1$ and $v_w = 1$ does not affect the result of percolation since it is independent of scaling, so if we scale volume in terms of $v_w t_{growth}$ the number of bubbles in the said volume stays constant when changing v_w or Γ_f. Then with a fixed Γ_f, the value of β can be acquired from Eq. (2.14). We can then compare the theoretical $h(t)$ as given by Eq. (2.16) to the simulated number of bubbles N per final (simulated) number of bubbles N_f which should follow the theoretical $h(t)$ closely [12]. Note that the JMAK equation requires that the size of the bubbles be small enough compared to the volume [5].

In order to adapt this algorithm for the slow nucleation rate case, which is in conformal comoving coordinates, we first calculate the probability of no bubbles nucleating between times η_1, η_2 as

$$p(\eta_1, \eta_2) = \exp\Big(-\int_{\eta_1}^{\eta_2} V\Gamma_0 a(\eta)^4 d\eta\Big) = \exp\left(-\frac{1}{3}\frac{\Gamma_0}{H^4} V(\frac{1}{\eta_1^3} - \frac{1}{\eta_2^3})\right) \tag{3.5}$$

where V is now the comoving volume. Solving the equation $p(\eta_1, \eta_2) = r$, where r is the random number mentioned earlier, gives us the next nucleation time as

$$\eta_2 = \left(\frac{1}{\eta_1^3} + 3\frac{1}{V}\frac{H^4}{\Gamma_0}\ln(r)\right)^{-\frac{1}{3}}. \tag{3.6}$$

Other than this we need to modify the starting time of the simulation to be $\eta_1 = -1/H$; and if we use units of $H\eta$, simply $\eta_1 = -1$. We will also need to change the bubble growth between time steps to be $\Delta r = \eta_2 - \eta_1$. We can use this method for various phase transitions, as long as the nucleation rate can be well defined, by modifying the coordinates and probability of no bubbles nucleating between two times.

3.3 Detecting percolation

In order to check whether or not we have percolation, we need a way to find connected regions of bubbles. We will employ a simple algorithm that starts from a random bubble and checks for bubbles that touch this bubble. If such bubbles are found, we repeat the same each found bubble until we cannot find any more bubbles that touch the last one. This is the main algorithm utilized in finding the percolating cluster. However, there are also some alternative approaches, for example, by the use of surface points [26] or by discretizing the spheres [27]. Another possible approach is to add bubbles to their corresponding clusters as we place them during the nucleation algorithm. However, we expect that this may not be as fast since we want to simulate the volume up to some time t and we do not really need to know about the status of the system before this.

The following algorithm we will describe is likely less optimized than the other methods found in the literature and our results seem to indicate that it is also less accurate. However, this algorithm can function separately from the bubble placement algorithm. There is likely also further optimization that can be done to this method. The starting point of the algorithm is when we already have placed the bubbles and we want to check if the configuration of the bubbles we have percolates.

To find the clusters, we employ a method similar to the depth-first search algorithm found, for example, in [34]. We start from some bubble in the volume that we have not yet visited. We check the neighboring cells for bubbles that touch this bubble. If we find any, we put them into a dedicated array, which we call a stack. While we have bubbles in the stack, we keep looping through the bubbles in the stack and search for bubbles that touch the bubble we are currently looking at, while removing it from the stack. When the stack is empty, we have found a cluster of bubbles. As we might have very complicated overlaps, we should only check the bubbles which we have not visited at all and which are not in the stack. The pseudocode for this algorithm is as follows.

Algorithm 2 An algorithm for finding clusters of bubbles

```
for each bubble b in the system do
    set b as current bubble b_c
    add b into stack
    while stack has bubbles do
        set last bubble in stack as b_c
        mark b = b_c as visited and in stack
        add b_c to a cluster c
        for each neighbor bubble b_n in each neighboring in cells do
            if bubbles b_n and b_c overlap then
                if b_n is not in stack and not visited then
                    Add b_n to stack
                end if
            end if
        end for
    end while
    if the latest found cluster c percolates then
        update whatever relevant statistics like number of successes
        exit loop
    end if
end for
```

At this point on lines 8 and 9 we do not check the cells on the other side of the volume or include periodic boundaries, as this would complicate the algorithm. Instead, we can consider those during the percolation check, which we will turn our attention to next.

3.3.1 Percolation Check

We now describe the algorithm for checking whether the cluster wraps around the volume, in other words we check whether we can cross the volume through it. When simulating a finite volume, we have a choice of criteria for percolation. In other words, do we require that the percolating cluster wraps around along one specific axis, all axes, or any of the axes? It turns out that the final result for the critical threshold in the infinite-volume limit does not depend on how we choose the criteria [27]. As such, we only check that the cluster wraps around along any of the three main axes, which we found to make the finite-scaling fit more accurate. To check that a cluster wraps around a certain direction, say along x-axis, we first find bubbles in the cluster that intersects the boundary at $x = 0$. Now we move the boundary on the opposite side equal to the amount the first bubble extends beyond the $x = 0$ boundary. Then we start looping through all the bubbles in the cluster to find one that intersects this moved boundary and overlaps the first bubble with the periodic boundaries taken into account. We must also check if we have a bubble intersecting the boundary at $x = L$, in which case we move the $x = 0$ boundary. If the conditions for either of these cases are met in any direction, we have a cluster that wraps around the volume.

Note that there is likely a much better algorithm for doing this, as currently we waste iterations on looking for a specific condition in, say y direction, that we could have accidentally stumbled upon while looking for a percolation x direction. However, this is not the slowest part of the simulation code. Additionally, one could possibly get away without considering periodic boundaries as the contribution at best is an effect that goes away for larger volumes/smaller bubbles. Removing the periodic boundaries would make finding the percolating cluster a trivial check for whether there exists a bubble in the cluster that crosses both boundaries. As a final side note, one can extract approximately the number of collisions by counting the number of clusters with two or more bubbles and then numerically differentiating respect to time.

The percolation check as pseudocode is given in Algorithm 3. We will note $\vec{b_c}$ as the location of the bubble center with $b_c^i, i = 1, 2, 3$ as the components and $|b_c|$ as its radius, and $D_s()$ as the function for the shortest distance, Algorithm 1. Additionally, we note P_0^i as a boolean variable for whether boundary at $x = 0$ in the coordinate direction $i = 1, 2, 3$ is intersected, similarly P_L^i for the boundary at L.

Algorithm 3 An algorithm for percolation check

for all bubbles b_c in cluster c **do**
  for $i = 1, 2, 3$ **do**
    if $b_c^i - |b_c| \leq 0$ **and** $\neg P_0^i$ **then**
      $P_0^i \leftarrow$ true
      for all bubbles b_p in cluster c **do**
        if $b_p^i + |b_p| \geq L - (|b_c| - b_c^i)$ **and** $D_s(\vec{b_c}, \vec{b_p}) < |b_c| + |b_p|$ **then**
          $P_L^i \leftarrow$ true
          exit
        end if
      end for
    end if
    if $b_c^i + |b_c| \geq L$ and $\neg P_L^i$ **then**
      $P_L^i \leftarrow$ true
      for all bubbles b_p in cluster c **do**
        if $b_p^i - |b_p| \leq |b_c| + b_c^i - L$ **and** $D_s(\vec{b_c}, \vec{b_p}) < |b_c| + |b_p|$ **then**
          $P_L^0 \leftarrow$ true
          exit
        end if
      end for
    end if
  end for
  if P_L^i **and** P_0^i for any $i = 1, 2, 3$ **then**
    cluster c is percolating cluster
    exit
  end if
end for

3.4 Limitations

Finding the critical fractional volume ϕ_c via this method is not the fastest as we need many repeat simulations since percolation and nucleation are stochastic processes and, in addition, for the slow transition the simulation becomes exponentially slower as we approach $\eta = 0$ for small values of Γ_0/H^4. For the fast transition and for $\Gamma_0/H^4 \gtrsim 1$, the simulation is sufficiently fast such that we are able to do in order of $10^2 - 10^3$ trials in a reasonable time. The simulation, even in the fast case, slows down when we approach $h(t) = 0$ as it becomes increasingly unlikely to find an empty spot in the volume to place a bubble. As such, one should carefully consider the times to simulate and when to terminate the simulation.

For the simulation to be as accurate as possible we require a large enough volume, not only because of the assumption from the JMAK equation, but we also need to be at a large enough scale to see the clusters. This causes issues for the slow transition as the scale factor tends to infinity at $\eta = 0$. Even if we start with a small volume, it quickly becomes too large for the simulation to handle due to the exponential increase in the number of bubbles. How quickly the simulation becomes too slow for us to handle depends on Γ_0/H^4 for the slow transition.

Lastly we hypothesize that while we can detect percolation we might not be able to rule out non-percolation due to the nature of looking at a finite volume. A pathological example of this would be that on average the clusters reach a very large finite size while being larger than the volumes we have simulated. In such a case, if possible, we would get a false positive result. However, we might notice discrepancies with the finite-size scaling. This potential false positive is something that would need further investigation, as it might also be a non-issue in most cases due to the homogeneity and statistical nature of the problem. As a result, we were unable to determine when percolation does not occur. Further compounded by the fact that the simulation becomes too slow for $\Gamma_0/H^4 \ll 1$. Although we can question a positive result, a negative result from a smaller volume would likely be conclusive. If no percolating cluster ever forms in a limited volume, we should not expect it to form in the infinite-volume limit.

4. Implementation

Now we will describe the implementation of the simulation as code and some specific methods that were used for the chosen languages `Fortran` and `Python`. `Fortran` was used for the simulation itself and `Python` for data analysis and calling the `Fortran` program. We also describe our approach to the error approximation and finally test the method against the known result of $\phi_c \approx 0.2895$ for equal-sized randomly distributed spheres.

We first summarize the simulation steps needed to obtain the estimate of the critical fractional volume ϕ_c as follows.

1. Start from some volume L^3 which to simulate. We seek a way to estimate the probability of percolation p as a function of time or fractional volume. We get an estimate of the probability at some time as $p = N_s/N$, where N is the number of trials and N_s the number of successes out of these as described in Sec. 4.2.

2. Gather data points around the time when percolation should occur, ideally around the probability of percolation $p \sim 0.5$ for the best error approximation as described in the aforementioned section.

3. Fit the function of Eq. (2.10) into the data points to get the value for $\phi_c(L)$.

4. Increase the volume size and repeat to gather more data points for $\phi_c(L)$.

5. Finally, fit the finite-size scaling of Eq. (2.9) to find the final value ϕ_c.

4.1 The code

The simulation code was made in the `Fortran` language, with additional libraries for the Mersenne-Twister random number generator (RNG) [35, 36] and `OpenMP` for multiprocessing, which is included in the GNU Fortran compiler[†]. For compilation, the GNU Fortran compiler `gfortran` version 14.3.1 20250523 was used. For data fitting with `Python` the `SciPy` [37] package was used. The code will be made available on

[†] https://gcc.gnu.org/fortran/

GitHub sometime after the release of this thesis at https://github.com/phy-lasse/bubble-nucleation with some of the relevant graphs used in this thesis, the data and better documentation to be added later. We should also note that the code was not tested for Mac or Windows machines, and compilation might cause errors on some compiler versions. The compilation of code itself is done by calling `gfortran` as

```
gfortran -O3 [<source code file>] -o program.o -fopenmp
```

where `-O3` flag sets the optimization level to 3. For debugging, the flags `-g -fbacktrace` can be included. After compilation, the program can be called via the command line. For the fast transition version, the usage when the compiled program `program.o` is in the working directory is

```
./program.o [<tau_f>] [<G_f>] [<L>] [<repeats>] [<threads>]
```

where `tau_f` is the τ value that ends the simulation, `G_f` is the Γ_f value and `L` is the boundary size L. Repeats N_r and the number of processor threads to use N_t set the total number of trials $N = N_r N_t$.

We also include versions for the slow transition and equal-size spheres. The usage of these is the same as before, apart from the different input parameters. For the simulation of equal-size spheres, `tau_f` is replaced by ϕ and `G_f` by the radius of the bubbles. For the slow transition simulation, the usage is

```
./program.o [<eta_f>] [<G_0>] [<L>] [<repeats>] [<threads>] [<H>] [<N_f>]
```

where `eta_f` is the final η, `G_0` is Γ_0 and so on, the two new parameters `H,N_f` are the Hubble constant and the final number of bubbles N_f. The `N_f` parameter is only used to allocate the arrays. This is estimated or calculated from Eq. (2.40). We use the method `scipy.integrate.quad` to numerically evaluate the integral.

Finally, in order to get the number of bubbles as is done in Sec. 4.3.1, we simply print the number of bubbles `N_bub` if we add a new bubble to the volume. For the most part, we used IO redirection in the Linux terminal >,>> to save the data to files.

Random Number Generation

For the random number generator, we use the Mersenne Twister (MT) made available from [36]. Specifically, we use the code by Richard Woloshyn as we got this to work the best. As we need to do multiple repetitions, we use multi-threading running N_r repeats on each N_t threads, we also want to make sure that the we seed the RNG properly, this was done reading a seed from `/dev/urandom` on a Linux machine. We should note that `/dev/urandom` tends to be less random than `/dev/random/` if called too fast if the system does not have enough time to gather entropy [38]. However, as

we only seed the RNG for each thread when we call the `Fortran` code, we expect there to be enough time to gather enough entropy in between runs. The period of MT is very long—at around $2^{19937}+1$ [35]—so we should not have an issue with the RNG repeating itself for longer runs.

We should mention that due to some quirks we were unable to solve, we merged the MT code into the main code in order to obtain a unique seed for each thread. There is probably a nicer way of implementing this, but to our knowledge, this is an adequate fix. We also had to clamp the randomly generated positions within the volume to not include location on the boundary L as this caused issues with placing bubbles into the cells. We did this by taking the minimum of the random location and $L-10^{-10}$, which should have a negligible effect on the total accuracy of the simulation.

Data Fitting

For fitting the finite-size scaling law Eq. (2.9) and Eq. (2.10) into our data, we use the `SciPy` library, specifically the method `scipy.optimize.curve_fit`. We use `absolute_sigma=True` and the error Eq. (4.4) as the `sigma` value. The fit error in this case is given by the square root of the diagonal of the resulting covariance matrix that the method gives. This fit error for the parameter $\phi_c(L)$ is then used to fit the finite-size law to our data, from which the final value of ϕ_c and its associated fit error are obtained.

Additional notes on the Code

We note some of the `Fortran` derived types used in the code, as these highlight details on the way we implement the methods described in Sec. 3. The derived type `bubble` which we use to represent the bubbles. The bubbles have a real-valued 4-array that contains the coordinates and the radius. In addition, they have an integer-valued 3-array for the coordinates of the cell the bubble resides in. Lastly, we have two boolean values used to keep track if the bubble is in the stack and if we have already visited it.

Next we have the type `bub_array` which is just a pointer of type `bubble`. This is used in the types `cells` and `bstack`, which is the stack used in the cluster finding algorithm described in Sec. 3.3. Cells also have an integer that counts the number of bubbles in the cell. Note that for the allocation of the relevant arrays we have used the value of $3N_f$ (for the cells $3N_f/N_{cells}$). This can be better optimized for smaller memory usage if necessary.

As an example of how these are used, we will describe how the bubbles are added to the simulation with the subroutine `add_new_bubble`. We have a counter `N_bub` that keeps track of the total number of bubbles, this gets trivially increased by 1 when we call

the subroutine. Next, we allocate space for a new `bubble` in the `bubble_array_deb`, which is of type `bstack` and is the main array where the bubbles are stored. Next, for the new bubble in the array we set all the variables used in the type `bubble`. We then allocate space in the cell's `bub_array` for storing bubbles–this is the array of pointers. We should note that we tried to do this before adding bubbles, but found this to be faster for reasons unknown to us. Finally, we assign the value for a pointer in the cell's `bub_array` to point to the added bubble in the main array `bubble_array_deb`. Similarly, pointers are used to assign the current bubble we are looking at during the cluster finding process.

4.2 Error approximation

For each system size L and fractional volume h we have some probability p for percolation. We only have two possibilities; percolation P and non-percolation $\neg P$. As such, let the random variable X be

$$X = \begin{cases} 1, & \text{if } P \\ 0, & \text{if } \neg P \end{cases} \tag{4.1}$$

When determining whether percolation occurs, we are asking N simple yes or no question. These are known as Bernoulli trials. One might expect this to be directly a binomial distribution, but the issue is that due to the very stochastic nature of the problem, we are unsure whether p itself has some distribution*. This detail would complicate the error analysis as the assumption of binomial distribution is not entirely valid. However, this would likely only add variance to the distribution of X. As such, we expect that any error analysis based on this assumption underestimates the error in the measured probability $\hat{p}$ defined below. These effects could be further studied in the future if one wants to improve the error estimates.

We assume that this distribution has a well-defined mean μ and variance σ, such that the Central Limit Theorem can be applied. Then from the Central Limit Theorem, we should that the sample average $\bar{X}$ is normally distributed with standard deviation $\sigma/\sqrt{N}$ and mean μ, as such we can find some probability $\hat{p} = \bar{X}/N$. So, even if p itself is distributed, we can still find a meaningful representative for the percolation probability as a function of L and h, which approaches a step function in the limit of $L \to \infty$.

Now we can focus on the error analysis, for which we use the Wilson score interval [39, 40]. The Wilson score interval assumes that there exists some true probability p which we are trying to measure with N trials as $\hat{p} \equiv N_s/N$, where N_s is the number

*We suspect that this would fall under so called beta-binomial distribution.

of successes. In other words, we assume that our random variable $\hat{p} \sim \text{Bin}(N, p)$, or that N_s is binomially distributed, which in our case is $N_s = \bar{X}$ and that we can approximate it with a normal distribution. As such, we assume that $np(1-p)$ is large enough that we can approximate X as normal, which should be a good approximation when $np \geq 10, n(1-p) \geq 10$ [40]. As we aim for around $p \approx 0.5$ with trials in the range of several hundreds, this should be sufficient.

For the normal approximation, if we knew the true probability p we could calculate the standard deviation $\sigma = \sqrt{p(1-p)/n}$ and the confidence interval $(p - z_{\alpha/2}\sigma, p + z_{\alpha/2}\sigma)$ for the sample $\hat{p}$. Now consider the probability of $\hat{p}$ lying in this interval with confidence $1-\alpha$, it is given by the normal distribution as

$$P\left(p - z_{\alpha/2}\sqrt{p(1-p)/n} < \hat{p} < p + z_{\alpha/2}\sqrt{p(1-p)/n}\right) = 1 - \alpha. \tag{4.2}$$

This also defines the confidence interval. Solving the inequality for p in the argument gives us [39, 40]:

$$p_{\pm} = \frac{1}{1 + z_{\alpha/2}^2/n}\left(\left(\hat{p} + \frac{z_{\alpha/2}^2}{2}\right) \pm \frac{z_{\alpha/2}}{2n}\sqrt{4n\hat{p}(1-\hat{p}) + z_{\alpha/2}^2}\right). \tag{4.3}$$

This is known as the Wilson score interval. We will use this to estimate the error. However, this interval is heavily asymmetric further we go from $\hat{p} = 0.5$, which is something to keep in mind when performing the fitting to the data. We can get away with not accounting for this when we are near $\hat{p} \sim 0.5$ and especially for a large number of repeat trials N.

As such, to simplify things, we will aim for values of $\hat{p} \sim 0.5$ in our simulation and we will estimate the error to be

$$\sigma \approx \max\left(\hat{p} - p_-, p_+ - \hat{p}\right) \tag{4.4}$$

with $\alpha = 1 - 0.69$, which will give the value for a 69% confidence interval, which is, for a good measure, slightly larger than 1σ for the normal distribution. This should give an approximation for the error near $\hat{p} \sim 0.5$. We should also note that the error is likely underestimated for smaller volumes and possibly for a low number of trials. For small volumes, a single addition of a bubble might cause percolation to occur, as such we expect there to be bigger variance in the result that is not accounted for, and a full picture of the error estimate would need a way of accounting for the finite-size effects.

4.2.1 Bootstrap Estimate for the Standard Deviation

We will be using bootstrap resampling to estimate a confidence interval for the standard deviation σ based on the data, in order to gauge whether Eq. (4.4) is believable.

The basic methodology of bootstrap is as follows [40, 41].

1. Generate B bootstrap samples x^* by drawing with replacement from the original sample x.

2. For each bootstrap sample x^* we calculate the standard deviation $\sigma(x^*)$ of the sample.

3. We store these into an array which gives us the bootstrap replication of the distribution for σ

4. We sort the values in the array and finally take confidence interval $1 - \alpha$ to be $(B\alpha/2)$th and $B(1 - \alpha/2)$th value of the resulting bootstrap distribution.

We will assume that the standard deviation is independent of time τ and the size of the system L. We expect that this might not be completely valid, but it should give us an indication of whether our error estimate is realistic. Note that the number of trials might also play a role in this. The issue is that testing multiple configurations is not realistic, as we would need to vary three parameters τ, L, N for a more complete analysis. Additionally, we would need to vary one more addition parameter, Γ_0/H^4, in the slow transition case.

We will use a boundary size of $L = 29$, two different trial counts $N = 9600$ and $N = 110$, and a final time of $\tau_f = -1$ for fast transition simulation. For $N = 110$, we performed 1000 simulations, and for $N = 9600$ we performed 100. From each data set, we calculate the mean standard deviation $\bar{\sigma}$ as given by our error approximation Eq. (4.4) and also its standard deviation σ_s. Then we perform the bootstrap method for $B = 10000$ and calculate the mean of the bootstrap estimated standard deviation $\bar{\sigma}^*$ and the confidence interval (CI) estimate for $\bar{\sigma}$. If we are within the 95% CI, it would indicate that our error estimate has some merit. We also include a sample standard deviation s for the probability. The results of the bootstrap estimate are in Table 4.1.

We can see that even for $N = 110$ we are within the 95% CI, as such our error approximation likely gives a result in the right order of magnitude. We also note that this method might be usable in estimating the percolation probability p, which could possibly make the simulation faster as we could use fewer number of trials N.

N	Samples	s	$\bar{\sigma}$	σ_s	$\bar{\sigma}^*$	CI 95%
110	1000	$5.128 \cdot 10^{-3}$	$5.177 \cdot 10^{-3}$	$2.652 \cdot 10^{-6}$	$5.088 \cdot 10^{-3}$	$(4.403, 5.757) \cdot 10^{-3}$
9600	100	$4.934 \cdot 10^{-2}$	$5.063 \cdot 10^{-2}$	$2.084 \cdot 10^{-4}$	$4.931 \cdot 10^{-2}$	$(4.706, 5.152) \cdot 10^{-2}$

Table 4.1: Result of the bootstrap estimation with $B = 10000$ for the standard deviation of the percolation probability for $\tau_f = -1$ and $L = 29$ for the fast transition simulation. Where N is number of Bernoulli trials, s the sample standard deviation, $\bar{\sigma}$ mean of the error approximation we get from Eq. (4.4) and σ_s its standard deviation. Finally, $\bar{\sigma}^*$ is the bootstrap estimate for the average standard deviation and last column the 95% confidence interval. We can see that our error estimate falls within the confidence interval, indicating that it is at least a decent approximation. In fact we slightly overestimate the error, but this is better than an underestimation.

4.3 Testing the Simulation

We will now turn our attention to testing the methods described in Sec. 3.

4.3.1 Bubble Nucleation

Fast Transition

For the fast transition, we compare the simulated ratio N/N_f, where* N_f is the final number of bubbles in the simulation, to the fractional volume $h(t)$ as given by Eq. (2.16). We chose the volume to be $L^3 = 50^3$ and the termination time to be $\tau = 3$, and as described earlier, we had set $\Gamma_f = 1$. The simulation finished with $N_f = 55669$ on a Ryzen 5 3600 processor in roughly 30 minutes on a single thread. Plotting $h(t)$ and N/N_f against τ results in Fig. 4.1.

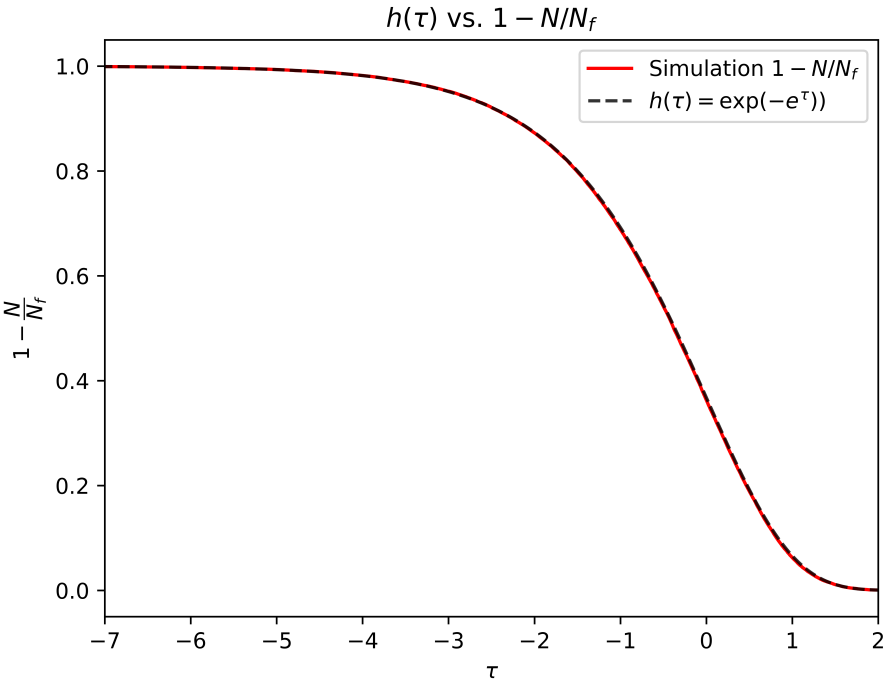

Figure 4.1: Plot of the $h(\tau)$ given by Eq. (2.16) and the simulated $1 - N/N_f$. This is the case as for the bubble volumes accounting for overlap goes as $V/V_f \propto N/N_f$. This also means that for the most accurate result $V_f \sim L^3$ is required. The maximum of the absolute difference between $h(\tau)$ and $1 - N/N_f$ was $\sim 5 \cdot 10^3$ here.

We can see that the simulation matches what we would expect from $h(\tau)$ very well, the absolute error here at worst was of the order $\sim 5 \cdot 10^3$, which when compared to

*Not to be confused with the final mean number of bubbles N_f from earlier.

N_f is quite small. However, we should note that this may partially be due to the usage of N/N_f instead of a more accurate metric for the fractional volume. The difference between the two graphs is sensitive to the value of N_f, and as such in Fig. 4.1 we use a very late value of $\tau = 3$ to obtain a more accurate N_f. Alternatively, one can also use the JMAK equation for the comparison as we will do for the slow transition.

Slow Transition

Since the physical volume diverges for $\eta = 0$, we are unable to obtain a reliable value for N_f in most cases. Instead, we calculate an estimate for the fractional volume h based on the JMAK equation Eq. (2.2) to compare to the $h(\eta)$ of Eq. (2.28). We first calculate the extended fractional volume of $\mathcal{V}_{\text{ext}}$ by summing the bubble volumes $4\pi r^3/3$ when we grow the bubbles. Note also that we only ran the simulation up to some $\eta < 0$, as it becomes increasingly slow for the late times. For boundary size $L = 20, H = 1$ and different values of Γ_0/H^4 we get the graph of Fig. 4.2.

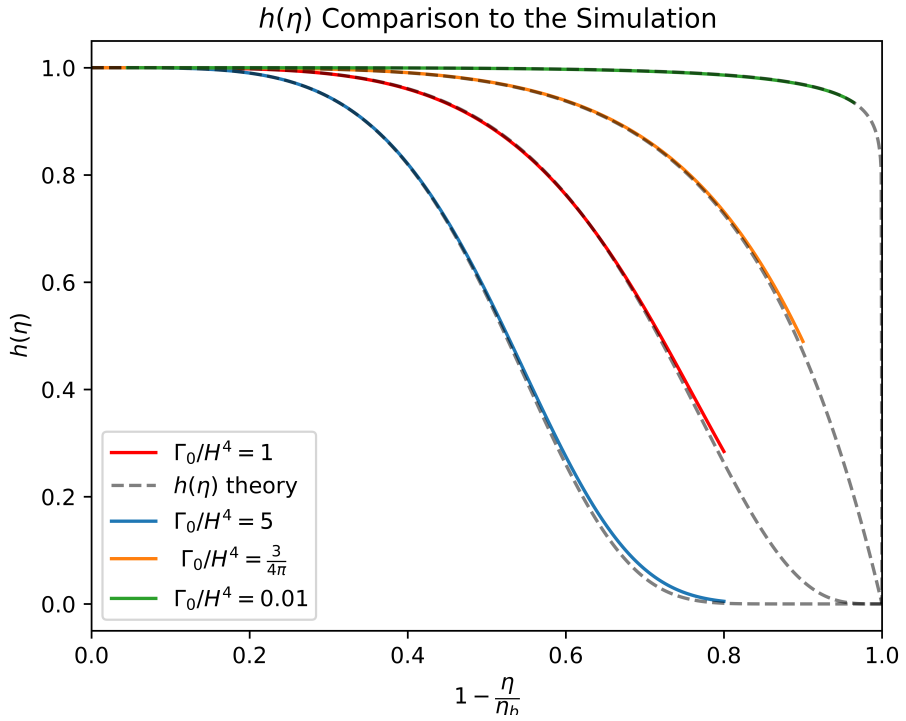

Figure 4.2: Result of fractional volume $h(\eta)$ from the simulation with $L = 20, H = 1$ for different Γ_0/H^4 values (colored lines) compared to the one given by Eq. (2.28) (the gray dashed lines). We can see that for $h(\eta) \sim 0.5$ and earlier the simulation follows the expected $h(\eta)$ very well, but for late times we consistently overshoot the expected values.

We are not sure what causes the deviation at late times from the expected $h(\eta)$. The simulation consistently overshoots once $h(\eta) \gtrsim 0.5$. This might be due to a small

mistake in the code, or floating point errors as at late times small bubbles might be more dominant. Right now we suspect it might be related to floating point errors during calculation of the nucleation times, as something likely overestimates or underestimates the size of the late time bubbles. Indicating perhaps that the nucleation times are more sparse or frequent than expected. We doubt that the issue is the bubble growing algorithm, as we checked that around the time the deviations start happening for $\Gamma_0/H^4 = 5$ as an example, the bubbles get increased by a radius in the order of 10^{-6}–10^{-8} and as the bubbles are at maximum of the order $r \sim 1$ this should not cause floating-point errors. We also tried different H values, which did not seem to fix this, but we should not expect an error here, as nothing explicitly depends on H alone in the fractional volume $h(\eta)$ or the simulation.

We should note that a similar trend occurs for the number of bubbles $N(\eta)$ compared to the numerically calculated mean number of bubbles from Eq. (2.40) as seen in Figure 4.3. We believe that since both $N(\eta)$ and $h(\eta)$ are overestimated after a certain point in time, it indicates that the problem is not present at early times. Since the number of bubbles $N(\eta)$ and the fractional volume $h(\eta)$ follow what we would expect from theory up to some time η, we have a reason to believe that bubble sizes or nucleation times start to deviate at late times. The deviation happens after we expect percolation to occur, and as such our simulation should be good enough despite this.

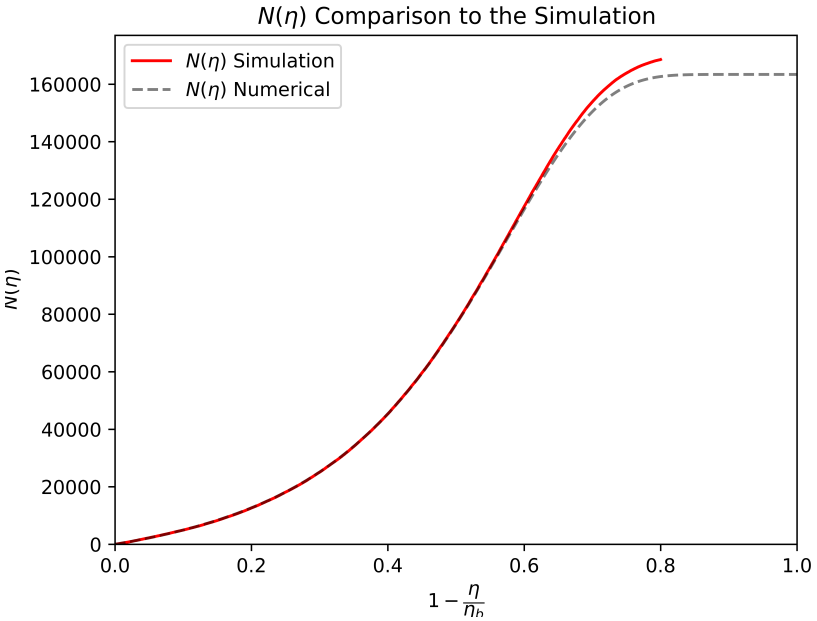

Figure 4.3: Comparison of the simulated $L = 20, \Gamma_0/H^4 = 5$ number of bubbles $N(\eta)$ against the one numerically calculated from Eq. (2.40) using quadratures. We can see that at late times we start to overshoot the one given by theory. In this case the absolute error was in the order of $\sim 5 \cdot 10^3$ at the time simulation was terminated $1 - \eta/\eta_f \approx 0.8$.

4.3.2 Percolation

We will now turn our attention to testing the simulation for finding the critical threshold ϕ_c for percolation. To do this, we will compare it against the known ϕ_c for equal-size uniformly distributed spheres. Currently, it appears that no analytical result has been found for ϕ_c in this case. There is some slight variance in the values of ϕ_c from different sources we could find, we have listed several of them in Table 4.2.

ϕ_c	Paper
0.2895693± 0.000 000 00026	[27]
0.289573± 0.000 002	[42]
0.28955± 0.00007	[24]
0.2896	[29]
0.290	[26]

Table 4.2: Table of different continuum percolation results for equal-size spheres.

We generate n spheres of fixed radius $r = 10$ in a volume of L^3. The number of spheres n is determined by solving n for a fixed fractional volume from the JMAK equation and taking the ceiling* of this value.

$$\phi = 1 - \exp\left(-\frac{4\pi}{3} n r^3 / L^3\right) \implies n = \left\lceil -\frac{3}{4\pi}\frac{L^3}{r^3}\ln(1-\phi) \right\rceil . \tag{4.5}$$

We note that this might introduce some additional error, since the relation between ϕ and n this way is not exact due to the statistical nature of the JMAK equation. However, for large enough volumes this difference should diminish.

Starting off, we will describe the issues that we found during testing. We believe that there may be an underestimation of the error and/or possibly some unaccounted systematic error. A systematic error shifts us away from the real value so that we still retain accuracy. If the error is underestimated, the sample variance we get from repeated testing differs from what the error estimate gives. Ideally we could just get the error estimate from the sample variance; however, in this case it is not fully realistic due to the time investment needed if done for large volumes which are needed for the most accurate result.

We describe a result that is acquired from a single simulation in Sec. 4.3.3 to highlight the basic idea of what is done, as the same fitting methodology is done later. For larger volumes and higher trial counts, we did a small number of simulation runs and get results that are consistent with each other. The largest issue is that we have two ways of getting the final result and these do not agree with each other. The first

*Floor would also suffice.

way to get the result is to directly fit the finite scaling law Eq. (2.9) to the $\phi_c(L)$, which we get by fitting Eq. (2.10) to the probabilities $p(\phi(L))$ for each boundary size L. The second way is to first use the scaling law for the width of the transition Eq. (2.11) to acquire the critical exponent ν—which is supposed to be around $\nu \approx 0.88$ [19, 20]—and then fit the finite-size scaling law with fixed ν value. The latter method consistently gives a result for ϕ_c that is of order 10^{-4} lower than the unfixed ν fit. We think this might indicate that the scaling law Eq. (2.9) has an exponent that is different form from what we expect. As such, in the end we chose to trust the value acquired with unfixed ν, but we also give the result for the fixed value. Finally, we note that the ν values of the fit match well with the results later in Section 5, indicating that even if we are making a systematic error, comparing the results is meaningful.

From a couple of simulation runs for a large number of trials and large volumes, we get the following data in Table 4.3. The fit error is quite sensitive to the data as sometimes `SciPy` was unable to give a fit error. In such a case, we added more data points or changed the initial guess `p_0` in the curve fit. We can see from Table 4.3 that the ν values are not quite compatible with each other in terms of error margins.

Trials	L	i	$\phi_c \pm \sigma_{fit}$	$\nu \pm \sigma_{fit}$	ΔL scaling $\nu \pm \sigma_{fit}$	$\phi_c \pm \sigma_{fit}$ fixed ν
9600	230–800	17	0.28927 ± 0.00004	0.38290 ± 0.03138	0.88183 ± 0.03047	0.28847 ± 0.00013
160000	250–750	13	0.28925 ± 0.00002	0.38533 ± 0.01322	0.96944 ± 0.00808	0.28837 ± 0.00010
160000	300–700	12	0.28925 ± 0.00002	0.37366 ± 0.02040	0.93138 ± 0.00901	0.28854 ± 0.00007
5000	270–700	10	0.28894 ± 0.00033	0.62669 ± 0.25105	0.94507 ± 0.04649	0.28849 ± 0.00007
10000	290–900	11	0.28926 ± 0.00005	0.36819 ± 0.05163	0.90239 ± 0.02629	0.28868 ± 0.00009
Σ	N/A	N/A	0.28919 ± 0.00037	0.42735 ± 0.28237	0.92602 ± 0.07158	0.28851 ± 0.00024

Table 4.3: Table of results from the three simulation runs. The first column is the number of trials N, second the range of boundary sizes used, third the number of data points i. Column ϕ_c is the fit with non-fixed ν and ΔL width scaling is the ν value acquired via fitting Eq. (2.11) and the last column is the ϕ_c value with the said ν value using the ODR method as described. Last row is the sample variance and sample σ. We didn't have time to further investigate the $N = 5000$ result and why it differs more significantly, we believe it might be due to the low number of trials or a statistical fluctuation. The final row is the sample average and standard deviation as described.

The final row in Table 4.3 is the sample mean and the standard deviation $\sqrt{\sum \sigma_i^2}$ of the data in the respective column. We calculate the standard error as the root of the sum of squares $\sqrt{\sum \sigma_i^2/N}$, where N is the number of samples, in this case $N = 5$. We also include the sample standard deviation in this calculation. As such, our final result as the sample mean and standard error is

$$\phi_c \pm \mathrm{SE} \approx 0.28919 \pm 0.00016 \tag{4.6}$$

Despite the possible inaccuracy, we believe that these results are consistent enough that we should be able to tell if there is a major difference in ϕ_c between the equal-size

spheres and the nucleation of bubbles in the phase transition. Compared to the known result $\phi \approx 0.2895$, we have a relative error of around ~ 0.0011 with the mean value, and the result is outside the margin of error. Finally, the critical exponent of column 5 of Table 4.3 is not what we would expect. As we stipulated earlier, this might be due to a systematic error, the quality of the data, or the exponent in the scaling law having a different form from what we expect.

We also mention that we had to rerun the simulation for some L, as we did not obtain any data between $p \in [0.35, 0.65]$ due to suboptimal time guesses. Thankfully, the simulations are all independent for different L and could be combined. We did not consciously pick data that made the fit better; instead we only discarded runs that gave no data in the aforementioned range, which we do not expect to cause a significant bias. We emphasize that this was due to the fact that it is not always trivial to get results in the correct range as the interval changes as we grow L.

4.3.3 Example of a Percolation Threshold Result

We will show an example of the data fitting procedure for the result in the first row of Table 4.3. Fitting Eq. (2.10) into the data for the boundary sizes $L = 230, 240, \ldots, 290, 300, 400, \ldots, 800$ is shown in Fig. 4.7 and Fig. 4.8. From these we get values $\phi(L)$ to which we fit the finite-size scaling law as shown in Fig. 4.4. We should note that we use cutoff to only select data with probability $p \in [0.35, 0.65]$ so as to be close to $p \approx 0.5$ as described earlier. For $N = 9600$, the confidence interval from the Wilson score is symmetric to values of order 10^{-4} near the edges of the interval $p \in [0.35, 0.65]$, thus the error we make is quite small.

From the covariance matrix we get the following values for the fit parameters ϕ_C, ν, A, where A is a constant factor.

$$\phi_c \approx 0.28927 \pm 0.00004, \quad \nu \approx 0.38290 \pm 0.03138, \quad A \approx 3688.0 \pm 4342.3 \tag{4.7}$$

This seemingly gives a decent value for ϕ_c however, the value of ν is not what we would expect. We can extract a value of ν closer to the known value $\nu \approx 0.88$ [19, 20] when we fit the scaling $\Delta L \propto L^{-1/\nu}$ to the data. The fit is done in Fig. 4.6 from which we get a good match to $\nu \approx 0.88$ as

$$\nu \approx 0.88183 \pm 0.03047 \tag{4.8}$$

This differs from the other results we obtained, and as such it is likely an outlier. However, some of the results also get close to this value, so it is likely that with more data we could obtain a result from the width scaling in agreement with what we expect.

We also have error in ν we need to propagate to our final result, this is done by defining a new parameter $x = L^{-1/\nu}$ then propagating the error from $\delta\nu$ to δx as

$$\delta x \approx \sqrt{\left(\frac{\partial(L^{-1/\nu})}{\partial\nu}\right)^2 \delta\nu^2} = \left| L^{-1/\nu} \frac{\ln(\nu)}{\nu^2} \delta v \right|. \tag{4.9}$$

Now, using the orthogonal distance regression (ODR) method in `SciPy` library we fit a function $p_c(L) = Ax + p_c$ to our data. With ODR we can account for the uncertainty in x and $p_c(L)$ data. This is done in Fig. 4.5 and we get

$$\phi_c \approx 0.28847 \pm 0.00013, \quad A \approx 1.4204 \pm 0.11758. \tag{4.10}$$

If the values of the error are to be trusted, we have a clear systematic error with this approach. It is likely that we would need more samples and a higher number of trials, but this would in turn take a lot more time to simulate.

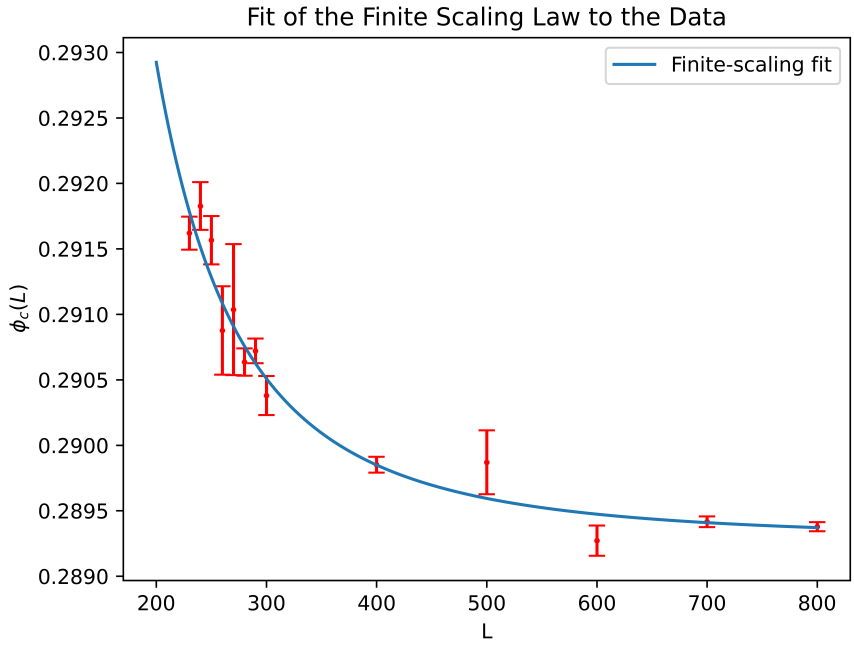

Figure 4.4: The $\phi_C(L)$ values acquired from fittings done in Fig. 4.7 fitted to the finite scaling law Eq. (2.9): $\phi = AL^{-1/\nu} + \phi_c$. From this fit we get the values in Eq. (4.7). We should note that even after some reruns the values did not significantly change, so we feel comfortable in saying the final value is at least $\phi_c = 0.2892$ from this simulation. A better estimate might possibly be acquired from using higher number of trials N fits for even larger volumes, which would take considerably longer. The larger volume values are more important in determining the final ϕ_c value, however these also require high accuracy to be useful for very large volumes.

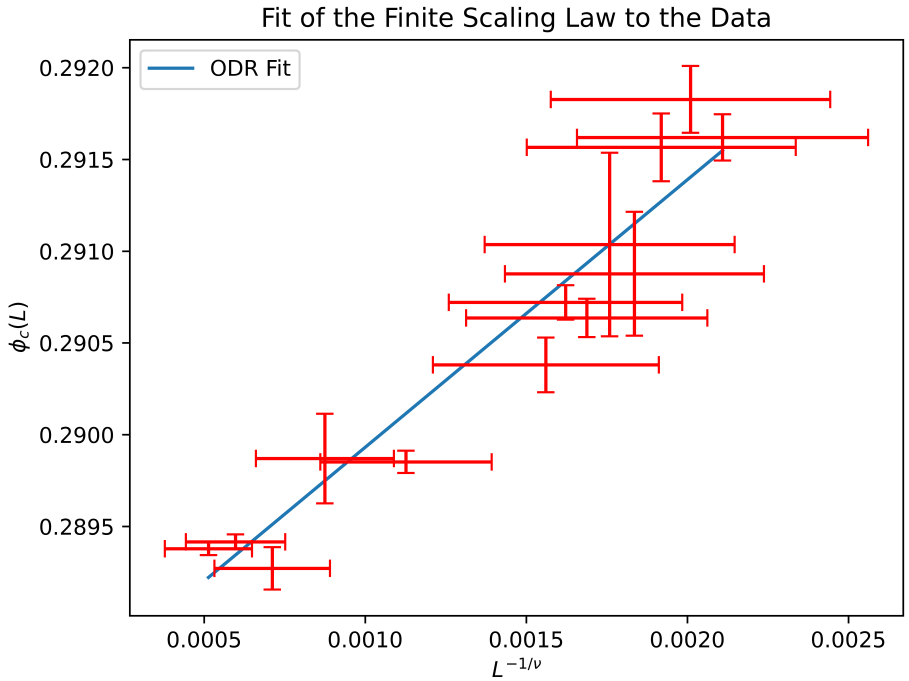

Figure 4.5: Fit of the data using ODR with fixed $\nu \approx 0.883$ value, this gives the results in Eq. (4.10).

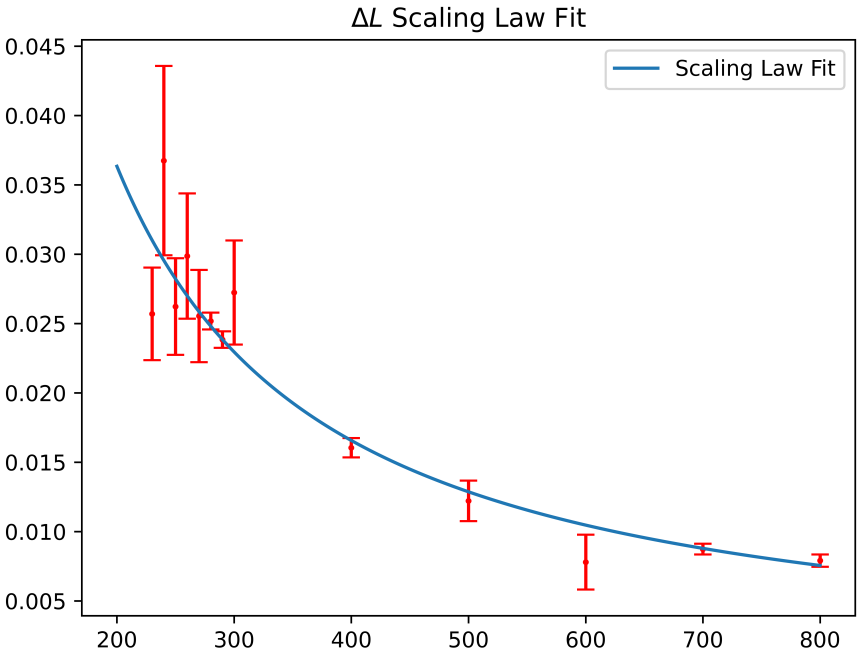

Figure 4.6: Fit of the scaling law $\Delta L \propto L^{-1/\nu}$ into the data, from this we acquired the result of $\nu \approx 0.88$ which was used in fitting done in Fig. 4.5.

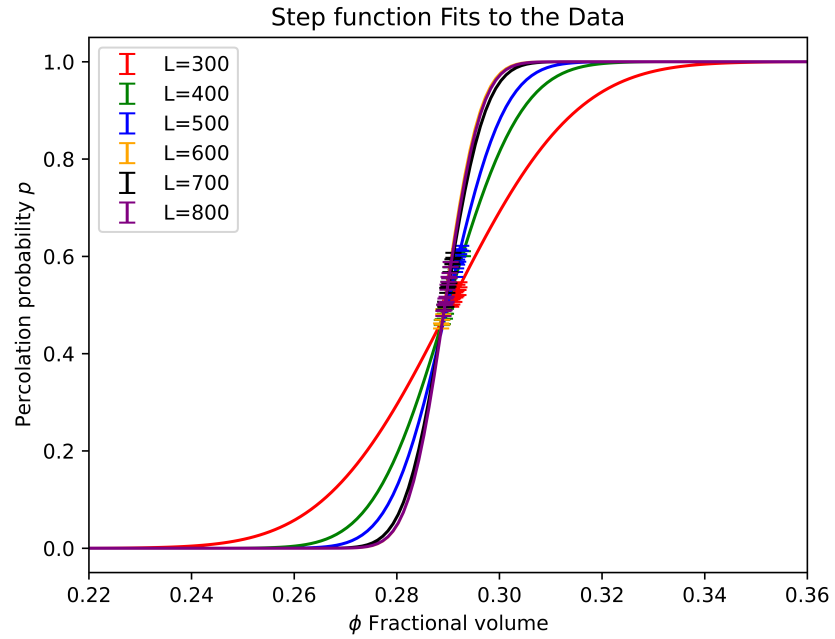

Figure 4.7: Resulting fits of Eq. (2.10) into some of our data points, which are near $p \sim 0.5$, such as we can better approximate the error as symmetric and gaussian. We can see that for larger volumes we approach a step function. Close up for $L = 300$ is in Fig. 4.8. For clarity we did not include data below $L = 200$, but they follow a similar trend. We should note though that the $L = 300$ fit is quite bad as $L = 290$ is slightly more converged towards the step function.

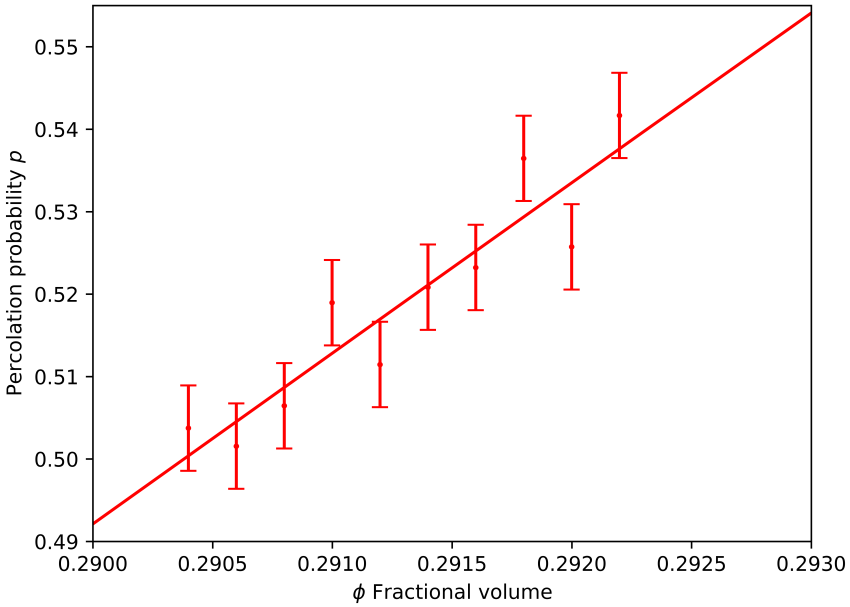

Figure 4.8: Close up of the fit of the step function Eq. (2.10) for $L = 300$ near the data points as seen in Fig. 4.7.

5. Results

We will now give the main results of this thesis, the critical fractional volume of bubbles ϕ_c for a fast and slow transition. In the case of a slow transition, we use the values $\Gamma_0/H^4 = 1, H = 1$. Setting $H = 1$ is a matter of fixing units, while Γ_0/H^4 is the parameter that controls the dynamics of the phase transition. Ideally we would try many different values for it, but as discussed in Sec. 3.4 this was deemed unrealistic for this thesis. Thus, we used $\Gamma_0/H^4 = 1$, which should be a complete transition based on the condition Eq. (2.34). Note that the results are likely dependent on the form of the nucleation rate. As an example, for the fast transition, the result applies if the nucleation rate is in the form of Eq. (2.13). As stated earlier in Sec. 3, we found a minor last minute error[†] in the implementation of the bubble nucleation code, which could affect the results slightly for smaller volumes. We should emphasize that this does not affect the result in Sec. 4.3.2. Note that the number of data points used for fitting the step function varied on the data we had available from the simulation.

5.1 Fast Transition

For the fast transition, using the same methodology as in Sec. 4.3.3, we get the result (5.2) based on five simulation runs listed in Table 5.1. Since $\phi_c \propto h_c \propto \exp(-e^{\tau})$ and the exponential function is monotonic, we can simply replace $\phi - \phi_c$ in the finite-size scaling law Eq. (2.9) with $\tau - \tau_c$. We have also included the scaling law fit with non-fixed ν in Figure 5.1 and the step function fit in Figure 5.2 for the run in the first row in Table 5.1.

The results are in the form of a critical $\tau_c = \beta^{-1}(t_c - t_f)$ value, as such we need to use Eq. (2.16) to calculate ϕ_c. As such, we have to propagate the error to ϕ_c:

$$\sigma \approx \left| \frac{\partial h(\tau_c)}{\partial \tau_c} \delta\tau_c \right| = e^{\tau_c} \exp(-e^{\tau_c}) \delta\tau_c. \tag{5.1}$$

[†]This has been fixed in the latest version found on Github.

Trials	L	i	$\tau_c \pm \sigma_{fit}$	$\nu \pm \sigma_{fit}$	ΔL scaling $\nu \pm \sigma_{fit}$	$\tau_c \pm \sigma_{fit}$ fixed ν
16000	40–90	7	-1.01432 ± 0.00050	0.36341 ± 0.04215	0.96789 ± 0.03879	-1.02188 ± 0.00119
9600	40–90	7	-1.01459 ± 0.00122	0.44086 ± 0.12014	1.00085 ± 0.06934	-1.02096 ± 0.00146
10000	25–45	5	-1.01232 ± 0.00370	0.40826 ± 0.10459	0.95673 ± 0.11192	-1.03457 ± 0.00295
17000	40–90	7	-1.01498 ± 0.00070	0.41524 ± 0.05807	0.97400 ± 0.03612	-1.02205 ± 0.00111
10000	25–70	13	-1.01347 ± 0.00117	0.42574 ± 0.04592	0.91223 ± 0.04024	-1.02638 ± 0.00169
Σ	N/A	N/A	-1.013936 ± 0.00429	0.410702 ± 0.18297	0.96234 ± 0.15103	-1.025168 ± 0.00695

Table 5.1: Table of results from the simulation runs, format is same as in Table 4.3. The first column is the number of trials N,i the number of data points, τ_c is the fit with non-fixed ν and ΔL width scaling is the ν value acquired via fitting Eq. (2.11) and the last column is the τ_c value with the said ν value using the ODR method as described in Sec. 4.3.3. Note that $\phi \approx 0.2895$ happens at $\tau \approx -1.0735$, so we have a clear difference from both the known result and the result we got in Sec. 4.3.3. Final row is the sample averages and the sample standard deviation for their respective columns. Note the ν values are comparable to that in Tables 4.3 and 5.2.

Performing this on the sample averages and sample standard deviations from column 2 in the last row of Table 5.1 and calculating the standard error gives us the result in Eq. (5.2).

$$\phi_c \pm \text{SE} \approx 0.30427 \pm 0.00048. \tag{5.2}$$

This result would indicate that the critical threshold is slightly higher for a fast transition as compared to the equal-size sphere result. We can do hypothesis testing to assess whether or not we should draw this conclusion [40]. Let the null hypothesis H_0 be that the equal-sized result $\phi_{c,equal}$ is the true result for the critical threshold in a fast transition $\phi_{c,fast}$, $H_0 : \phi_{c,equal} = \phi_{c,fast}$. We now ask whether we make a *type I error* if we were to reject H_0. The type I error would be if we reject H_0 despite it being true. We set a confidence level $\alpha = 0.05$, in other words, we are willing to risk that 5% the time we falsely reject H_0 when it was true. If hypothesis testing indicates that we rarely make a type I error when we reject the null hypothesis H_0, then it implies that we have strong evidence to favor the alternative hypothesis $H_a : \phi_{c,equal} \neq \phi_{c,fast}$.

We will assume that both $\phi_{c,fast}, \phi_{c,equal}$ follow the normal distribution with the standard deviations $s_{c,fast}, s_{c,equal}$. We then use the Welch's t-test, which uses the following test statistic [40]:

$$t = \frac{\bar{\phi}_{c,fast} - \bar{\phi}_{c,equal}}{\sqrt{s^2_{c,fast}/n + s^2_{c,equal}/m}} \tag{5.3}$$

where m, n are the number of samples, this approximately follows the t distribution. From the results 4.6 and 5.2, we have the values $se^2_{c,fast} = s^2_{c,fast}/n \approx 2.304 \cdot 10^{-7}$ and $se^2_{c,equal} \approx 2.56 \cdot 10^{-8}$.

For the given confidence level α, the rejection regions for H_0 are $t \geq t_{1-\alpha/2,\lambda}$ and $t \leq -t_{1-\alpha/2,\lambda}$, where λ is the degrees of freedom given by [40]:

$$\lambda = \frac{(s^2_{c,fast}/n + s^2_{c,equal}/m)^2}{\frac{(s^2_{c,fast}/n)^2}{n-1} + \frac{(s^2_{c,equal}/m)^2}{m-1}}. \tag{5.4}$$

Using this, we obtain the degrees of freedom $\nu \approx 4.878$. We now calculate the test statistic Eq. 5.3 from our data and check whether it falls into the rejection regions for H_0. We calculate the rejection regions with `scipy.stats.t`. The rejection regions and the test statistic are

$$t \approx 29.8, \quad t_{1-\alpha/2,\lambda} \approx 2.59. \tag{5.5}$$

Hence, as $t \geq 2.59$ we should reject H_0 in favor of the alternative hypothesis H_a that the values we have obtained are likely distinct from each other.

We can also calculate the p-value of our result by finding the maximal value for α when we no longer reject H_0. This represents the probability of obtaining a result as extreme as one obtained if we assume H_0 to be true. A lower p-value implies that, given our data, we should more likely reject H_0. Computing the p-value numerically, we obtain that

$$p \approx 1.0 \cdot 10^{-6}. \tag{5.6}$$

As such, we have strong evidence that our result is statistically different from the equal-size sphere result we got in Sec. 4.3.2. Even if we assumed a fixed ν value for the fast transition and an unfixed ν value for the equal-size spheres, which would make the difference between the results smaller, we still would get a p-value of $p \approx 10^{-4}$ and, as such we should still reject H_0 with $\alpha = 0.05$.

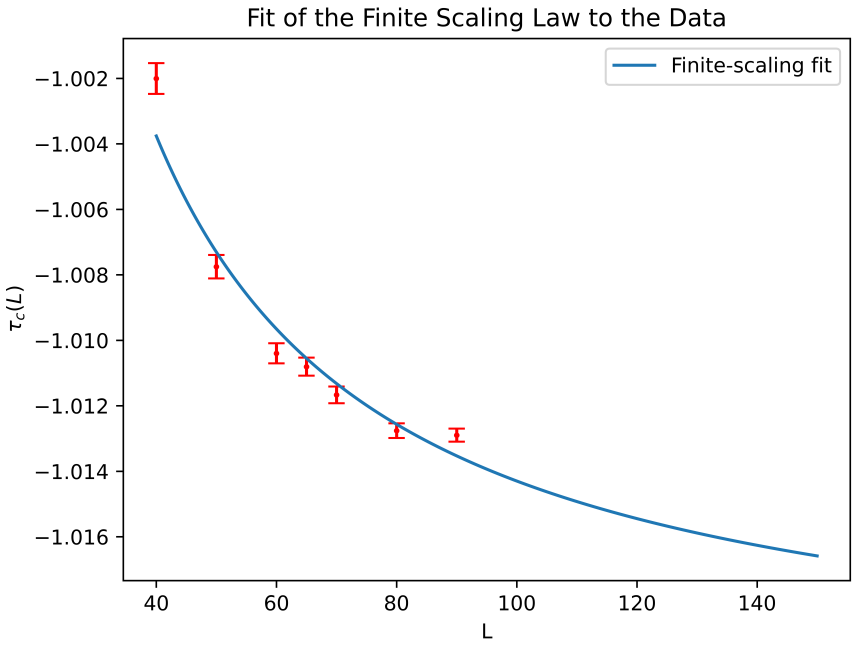

Figure 5.1: Fit of the finite-size scaling law Eq. (2.9) for a fast transition with trials $N = 16000$ corresponding to the first row in Table 5.1. We believe additional runs for $L > 90$ would be in order to see whether they also follow the fit as the data is quite limited. But, we doubt this would lower the ϕ_c/τ_c significantly enough to bring it closer to $\tau \approx -1.0735$, as we still got results within the expected range from the runs ending in $L = 45, L = 70$.

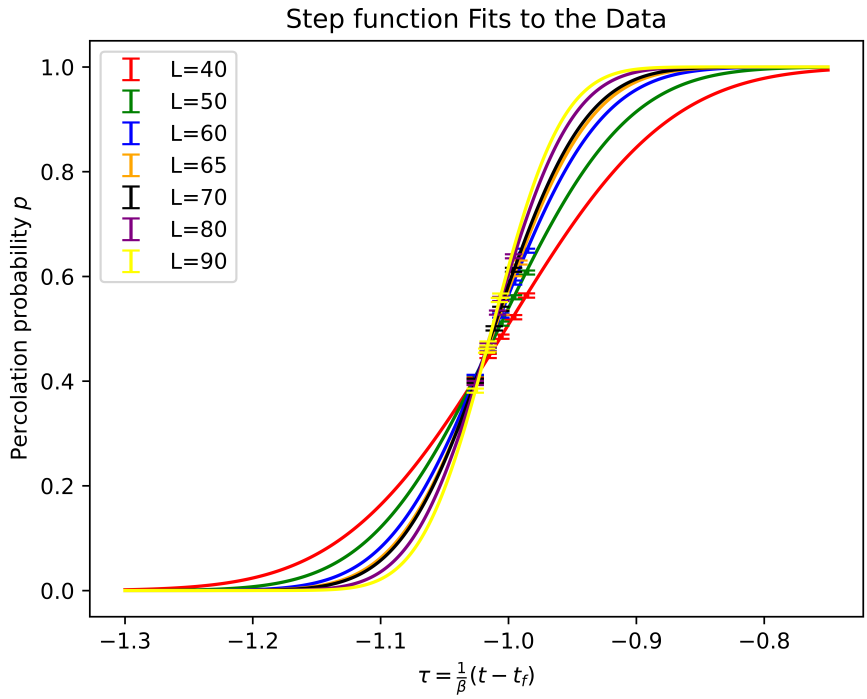

Figure 5.2: Fit of the step function Eq. (2.10) with the different boundary sizes for a fast transition.

5.2 Slow Transition

Similarly for the slow transition simulation with $\Gamma_0/H^4 = 1$, we obtain the data in Table 5.2.

Trials	L	i	η_c	ν	ΔL scaling ν	η_c fixed ν
13000	8–17	5	-0.36730 ± 0.00018	0.39972 ± 0.09328	0.91459 ± 0.04828	-0.36834 ± 0.00018
13000	8–17	5	-0.36760 ± 0.00047	0.60070 ± 0.22777	0.83236 ± 0.04265	-0.36807 ± 0.00007
12880	8–22	8	-0.36747 ± 0.00007	0.48999 ± 0.03985	0.97162 ± 0.02480	-0.36830 ± 0.00011
12800*	8–19	6	-0.36755 ± 0.00018	0.51932 ± 0.09919	0.89781 ± 0.03660	-0.36828 ± 0.00011
12800*	8–21	8	-0.36761 ± 0.00014	0.53686 ± 0.09510	0.94813 ± 0.03177	-0.36832 ± 0.00007
Σ	N/A	N/A	-0.36751 ± 0.00026	0.50932 ± 0.13149	0.91290 ± 0.04464	-0.36826 ± 0.00013

Table 5.2: Table of results from the five simulation runs for a slow transition. The data is organized in the same ways as in Table 5.1, expect for η being the time parameter now. Note the $*$ on the last two rows where have some data points done with 13000 trials instead of 12800, but such a small difference only affects the error estimate, for which we use the lower trial count. In this case $\phi_c \approx 0.2895$ happens at around $\eta \approx -0.3713$.

In the same manner as before, we perform error propagation, where the derivative is now given by expression in Eq. (2.31)

$$\sigma \approx \left|\frac{\partial h(\eta_c)}{\partial \eta_c}\delta\eta_c\right| = \left|\left(-\frac{4\pi}{3}\frac{\Gamma_0}{H^4}\left[\frac{\eta_c^2}{\eta_b^3} - 3\frac{\eta_c}{\eta_b^2} + \frac{3}{\eta_b} - \frac{1}{\eta_c}\right]\right) h(\eta_c)\delta\eta_c\right|. \tag{5.7}$$

Using this and Eq. (2.28), we obtain the following result:

$$\phi_c \pm \text{SE} \approx 0.29707 \pm 0.00053. \tag{5.8}$$

Performing the same hypothesis testing as earlier, we now have $\lambda \approx 4.723$, $t \approx 14.2$ and the rejection region $t_{1-\alpha/2,\lambda} \approx 2.63$ from Eqs. (5.3, 5.4). Thus, we find that for $\alpha = 0.05$ we should reject H_0 as the p-value is

$$p \approx 4.6 \cdot 10^{-5}. \tag{5.9}$$

This indicates a slightly less extreme result if we were to assume H_0 as compared to the fast transition, but still strongly indicates that we should reject H_0. As such, we expect that for $\Gamma_0/H^4 = 1$ the critical value is slightly lower than in the fast transition case and slightly higher than the result of the equal-size spheres. We are not yet sure whether this result is modified for different values of Γ_0/H^4, and based on the differences between the fast and slow transitions, we should expect there to be a dependence on Γ_0/H^4. We expect the distribution of sphere sizes, based on [24], and the distribution of nucleation centers to be parameters that determine ϕ_c.

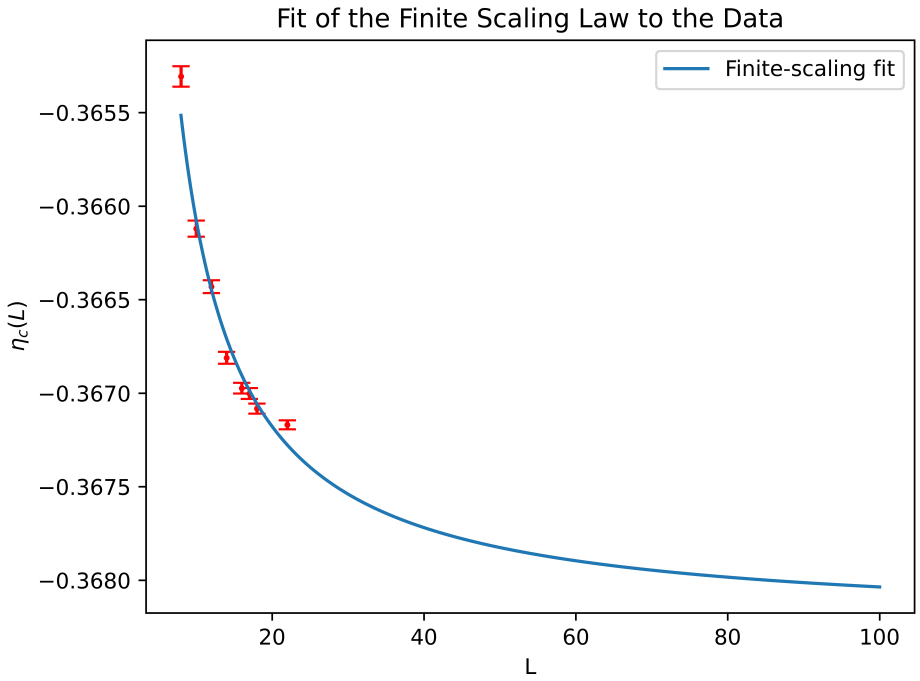

Figure 5.3: Fit of the finite-size scaling law for the third row in Table 5.2 with 12880 trials. As before, based on the fact that increasing the boundary size from 17 to 22 did not alter the result drastically, we doubt that the result would not be modified significantly to bring it closer to $\eta \approx -0.3713$. However, one should verify this for both cases by simulating even larger volumes, which we do not find realistic with the methods used in this thesis.

6. Discussion

In conclusion, if the Universe underwent a first-order phase transition at the EW scale, such an event would likely leave an imprint in the background gravitational wave spectrum that we could detect. Such a first-order phase transition proceeds via nucleation of growing bubbles of the new, broken symmetry phase of the Higgs field. As the transition progresses, the bubbles collide and coalesce, during which gravitational waves would be produced. In addition, depending on the expansion mode of the bubbles and the dynamics of the transition, the imprints from the collision of the bubble walls would continue to propagate, producing gravitational waves. Relevant to this process is the formation of an infinite cluster, or percolation, which is a necessary step for a complete transition. There exists a critical fractional volume ϕ_c that the bubbles must take up for percolation to occur, which we have determined numerically from our approximate simulation of a first-order phase transition. If the supercooling is very strong, the Universe could get stuck in the metastable phase such that the transition would never fully complete.

The results in Sections 5 and 4.3.2 indicate that for the fast transition as described in Sec. 2.3.1, the critical fractional volume of bubbles ϕ_c for percolation to occur is slightly larger $\phi \approx 0.3043 \pm 0.0005$ (Eq. (5.2)) compared to the commonly used equal-size sphere result $\phi_c \approx 0.2895$, for which we obtained $\phi_c \approx 0.2892 \pm 0.0002$ (Eq. (4.6)). In the case of the slow transition with $\Gamma_0/H^4 = 1$, we also find a slightly higher value $\phi_c \approx 0.2971 \pm 0.0005$ (Eq. (5.8)). As stated in Section 2.2.3, it is likely that neither of these results is universal for all cosmological phase transitions, since the distribution of bubble sizes and nucleation sites can differ depending on the model and parameters. Based on this, we should conclude that $\phi_c \approx 0.2895$ is likely a good approximation to use for the cases we examined in Section 2.3. We believe that this is likely true for many other models of cosmological transitions, but it should be verified on a case-by-case basis. We make some simplifying assumptions about the phase transition, which should be taken into account when applying these results.

We are left with some open questions which we leave for future work:

- Is the critical exponent ν in Eq. (2.9)?
- How is the critical value ϕ_c modified for different values Γ_0/H^4?
- What is the significance of the change in behavior of $h(\eta)$ around $\Gamma_0/H^4 \sim \frac{3}{4\pi}$
- When exactly does percolation cease to happen in the slow transition?
- How accurate is the error estimate of Eq. (4.4)?
- When are the assumptions of the JMAK Eq. (2.2) broken in cosmological phase transitions?
- How do we tell from the simulation if the phase transition does not complete?

The main significance of finding a critical value of percolation for Γ_0/H^4 would be to refine the result acquired in [7], where they found that there is a very narrow window of Γ_0/H^4 that could make the old inflation scenario possible. However, we are unsure of its significance for modern research besides better understanding a possible extremely supercooled transition. In order to answer when the slow transition percolates, we also must have a way to tell non-percolation from our simulation. We feel that developing methods for detecting non-percolation is the most significant question we are left with, as this would open the possibility for ruling out certain scenarios more easily. Another significant question is when does the JMAK equation no longer apply, as it is central to the analysis of the transition progress, especially in a supercooled scenario.

Lastly, examining the precision of Eq. (4.4) and whether the critical exponent is ν in Eq. (2.9) would help gauge the precision of the results of this thesis. In addition to this, the simulation itself could be further improved. Currently, we likely have some systematic error in our results, in addition to the simulation being too slow for some cases. As discussed in Sec. 3, the results might be slightly skewed from the minor mistake found in the code right that we did not have time to test the effects of.

For the slow transition, we found that we diverge from the expected value of $h(\eta)$ at late times in Sec. 4.3. We believe that we could reduce the number of trials used if the bootstrap method is incorporated by performing it for the random variable X of Eq. (4.1). Lastly, it is likely that a better overall method for generating the clusters could be found. One method that could be used is to focus only on the probability that the cluster will grow to a certain size. In such a case, we would only need to simulate the immediate region around the cluster on which we focus. However, such a method would require a complete overhaul of the methodology and additional theoretical considerations.

Usage of LLM tools

I acknowledge the use of an LLM in helping with the research during the course of this thesis. None of the text in this thesis has been generated with an AI, but Writefull* was used at times for general spell checking. Microsoft's Copilot and OpenAI's ChatGPT were used to search for research papers and to help with optimizing the code. We should mention that Algorithm 2 was refined from a suggestion made by ChatGPT.

*https://www.writefull.com/

Bibliography

[1] P. Auclair et al. "Cosmology with the laser interferometer space antenna". In: *Living Reviews in Relativity* 26.1 (2023). DOI: 10.1007/s41114-023-00045-2. arXiv: 2204.05434 [astro-ph.CO].

[2] P. Amaro-Seoane et al. "Laser interferometer space antenna". In: *arXiv Preprint* (2017). DOI: 10.48550/arXiv.1702.00786. arXiv: 1702.00786 [astro-ph.IM].

[3] M. B. Hindmarsh et al. "Phase transitions in the early universe". In: *SciPost Physics Lecture Notes* (2021). DOI: 10.21468/SciPostPhysLectNotes.24. arXiv: 2008.09136 [astro-ph].

[4] D. Croon and D. J. Weir. "Gravitational Waves from Phase Transitions". In: *Contemporary Physics* 65.2 (2024). DOI: 10.1080/00107514.2024.2423496. arXiv: 2410.21509 [hep-ph].

[5] P. Athron et al. "Cosmological phase transitions: from perturbative particle physics to gravitational waves". In: *Progress in Particle and Nuclear Physics* 135 (2024). DOI: 10.1016/j.ppnp.2023.104094. arXiv: 2305.02357 [hep-ph].

[6] G. A. White. *A Pedagogical Introduction to Electroweak Baryogenesis*. 2053-2571. Morgan Claypool Publishers, 2016. DOI: 10.1088/978-1-6817-4457-5.

[7] A. H. Guth and E. J. Weinberg. "Could the Universe Have Recovered from a Slow First Order Phase Transition?" In: *Nucl.Phys.B* 212 (1983). DOI: 10.1016/0550-3213(83)90307-3.

[8] J. Hirvonen. "Phase Transitions in Elementary-Particle Matter". PhD thesis. University of Helsinki, 2024.

[9] A. Linde. "Fate of the false vacuum at finite temperature: Theory and applications". In: *Physics Letters B* 100.1 (1981). DOI: 10.1016/0370-2693(81)90281-1.

[10] A. D. Linde. "Decay of the false vacuum at finite temperature". In: *Nuclear Physics B* 216.2 (1983). DOI: 10.1016/0550-3213(83)90293-6.

[11] R.-G. Cai, M. Sasaki, and S.-J. Wang. "The gravitational waves from the first-order phase transition with a dimension-six operator". In: *Journal of Cosmology and Astroparticle Physics* 2017.8 (2017). DOI: 10.1088/1475-7516/2017/08/004. arXiv: 1707.03001 [astro-ph].

[12] K. Enqvist et al. "Nucleation and bubble growth in a first-order cosmological electroweak phase transition". In: *Physical Review D* 45.10 (1992). DOI: 10.1103/PhysRevD.45.3415.

[13] J. Ellis et al. "Gravitational wave energy budget in strongly supercooled phase transitions". In: *Journal of Cosmology and Astroparticle Physics* 2019.6 (2019). DOI: 10.1088/1475-7516/2019/06/024. arXiv: 1903.09642 [hep-ph].

[14] P. Athron, C. Balázs, and L. Morris. "Supercool subtleties of cosmological phase transitions". In: *Journal of Cosmology and Astroparticle Physics* 2023.3 (2023). DOI: 10.1088/1475-7516/2023/03/006. arXiv: 2212.07559 [hep-ph].

[15] A. D. Linde. "Lectures on Inflationary Cosmology". In: *Lect. Notes Phys.* 455 (1995). Ed. by F. Occhionero. DOI: 10.1007/3-540-60024-8_130. arXiv: hep-th/9410082.

[16] J. Ellis, M. Lewicki, and J. M. No. "On the Maximal Strength of a First-Order Electroweak Phase Transition and its Gravitational Wave Signal". In: *Journal of Cosmology and Astroparticle Physics* 2019.4 (2019). DOI: 10.1088/1475-7516/2019/04/003. arXiv: 1809.08242 [hep-ph].

[17] A. H. Guth and E. J. Weinberg. "Cosmological consequences of a first-order phase transition in the SU_5 grand unified model". In: *Physical Review D* 23.4 (1981). DOI: 10.1103/PhysRevD.23.876.

[18] M. A. Ajmi and M. Hindmarsh. "Thermal suppression of bubble nucleation at first-order phase transitions in the early Universe". In: *Physical Review D* 106 (2). DOI: 10.1103/PhysRevD.106.023505. arXiv: 2205.04097 [gr-qc].

[19] D. Stauffer and A. Aharony. *Introduction to percolation theory*. 2nd revised. Taylor & Francis, 2003. DOI: 10.1201/9781315274386.

[20] M. Sahimi and A. G. Hunt, eds. *Complex Media and Percolation Theory*. Springer US, 2021. DOI: 10.1007/978-1-0716-1457-0.

[21] R. Meester and R. Roy. *Continuum Percolation*. Cambridge Tracts in Mathematics. Cambridge University Press, 1996. DOI: 10.1017/CBO9780511895357.

[22] J.-B. Gouéré. "Subcritical regimes in the Poisson Boolean model of continuum percolation". In: *The Annals of Probability* 36.4 (2008). DOI: 10.1214/07-AOP352.

[23] B. Bollobás and O. Riordan. *Percolation*. Cambridge University Press, 2006. DOI: 10.1017/CBO9781139167383.

[24] R. Consiglio et al. "Continuum percolation thresholds for mixtures of spheres of different sizes". In: *Physica A: Statistical Mechanics and its Applications* 319 (2003). DOI: 10.1016/S0378-4371(02)01501-7.

[25] M. Lewicki, P. Toczek, and V. Vaskonen. "Primordial black holes from strong first-order phase transitions". In: *Journal of High Energy Physics* 2023.92 (2023). DOI: 10.1007/JHEP09(2023)092.

[26] M. Li, H. Chen, and J. Lin. "Numerical study for the percolation threshold and transport properties of porous composites comprising non-centrosymmetrical superovoidal pores". In: *Computer Methods in Applied Mechanics and Engineering* 361 (2020). DOI: 10.1016/j.cma.2019.112815.

[27] P. Brzeski and G. Kondrat. "Percolation of hyperspheres in dimensions 3 to 5: from discrete to continuous". In: *Journal of Statistical Mechanics: Theory and Experiment* 2022.5 (2022). DOI: 10.1088/1742-5468/ac6519.

[28] J. Lin and H. Chen. "Continuum percolation of porous media via random packing of overlapping cube-like particles". In: *Theoretical and Applied Mechanics Letters* 8.5 (2018). DOI: 10.1016/j.taml.2018.05.007.

[29] J. Lin, H. Chen, and W. Xu. "Geometrical percolation threshold of congruent cuboidlike particles in overlapping particle systems". In: *Physical Review E* 98.1 (2018). DOI: 10.1103/PhysRevE.98.012134.

[30] M. S. Turner, E. J. Weinberg, and L. M. Widrow. "Bubble nucleation in first-order inflation and other cosmological phase transitions". In: *Physical Review D* 46.6 (1992). DOI: 10.1103/PhysRevD.46.2384.

[31] M. Maggiore. *Gravitational Waves: Volume 1: Theory and Experiments*. Oxford University Press, 2007. DOI: 10.1093/acprof:oso/9780198570745.001.0001.

[32] B. Abbott et al. "Observation of Gravitational Waves from a Binary Black Hole Merger". In: *Physical Review Letters* 116.6 (2016). DOI: 10.1103/physrevlett.116.061102.

[33] R. L. Streit. *The poisson point process*. Springer New York, 2010. DOI: 10.1007/978-1-4419-6923-1.

[34] R. Sedgewick and K. Wayne. *Algorithms*. Addison-Wesley professional, 2011.

[35] M. Matsumoto and T. Nishimura. "Mersenne twister: a 623-dimensionally equidistributed uniform pseudo-random number generator". In: *ACM Transactions on Modeling and Computer Simulation (TOMACS)* 8.1 (1998).

[36] *Mersenne-Twister code*. https://www.math.sci.hiroshima-u.ac.jp/m-mat/MT/VERSIONS/FORTRAN/fortran.html. Accessed: 2025-06-16.

[37] P. Virtanen et al. "SciPy 1.0: Fundamental Algorithms for Scientific Computing in Python". In: *Nature Methods* 17 (2020). DOI: 10.1038/s41592-019-0686-2.

[38] H. G. Katzgraber. "Random numbers in scientific computing: An introduction". In: *arXiv preprint* (2010). arXiv: 1005.4117 [physics.comp-ph].

[39] E. B. W. and. "Probable Inference, the Law of Succession, and Statistical Inference". In: *Journal of the American Statistical Association* 22.158 (1927). DOI: 10.1080/01621459.1927.10502953.

[40] J. L. Devore, K. N. Berk, and M. A. Carlton. *Modern mathematical statistics with applications*. 3rd. Springer Nature, 2021. DOI: 10.1007/978-1-4614-0391-3.

[41] B. Efron and R. J. Tibshirani. *An introduction to the bootstrap*. Chapman and Hall/CRC, 1994. DOI: 10.1201/9780429246593.

[42] C. D. Lorenz and R. M. Ziff. "Precise determination of the critical percolation threshold for the three-dimensional "Swiss cheese" model using a growth algorithm". In: *The Journal of Chemical Physics* 114.8 (2001). DOI: 10.1063/1.1338506.

Appendix A. Fractional Volume In a Slow Transition

For calculating the fractional volume we start from Eq. (2.27)

$$h(\eta) = \exp\left(-\frac{4\pi}{3}\int_{\eta_b}^{\eta}\Gamma_0\frac{1}{H^4\eta'^4}(\eta-\eta')^3 d\eta'\right). \tag{A.1}$$

Evaluating the integral gives

$$\int_{\eta_b}^{\eta}\frac{1}{\eta'^4}(\eta-\eta')^3 d\eta' = \int_{\eta_b}^{\eta}\frac{1}{\eta'^4}(\eta^3 - 3\eta'\eta^2 + 3\eta'^2\eta - \eta'^3)d\eta' \tag{A.2}$$

$$= \int_{\eta_b}^{\eta}(\frac{\eta^3}{\eta'^4} - 3\frac{\eta^2}{\eta'^3} + 3\frac{\eta}{\eta'^2} - \frac{1}{\eta'})d\eta' \tag{A.3}$$

this gives

$$= -\frac{1}{3}\eta^3(\eta^{-3} - \eta_b^{-3}) + \frac{3}{2}\eta^2(\eta^{-2} - \eta_b^{-2}) - 3\eta(\eta^{-1} - \eta_b^{-1}) - \ln\left(\frac{\eta}{\eta_b}\right) \tag{A.4}$$

$$= -\frac{1}{3}(1 - (\frac{\eta}{\eta_b})^3) + \frac{3}{2}(1 - (\frac{\eta}{\eta_b})^2) - 3(1 - (\frac{\eta}{\eta_b})) - \ln\left(\frac{\eta}{\eta_b}\right) \tag{A.5}$$

$$= \frac{1}{3}(\frac{\eta}{\eta_b})^3 - \frac{3}{2}(\frac{\eta}{\eta_b})^2 + 3\frac{\eta}{\eta_b} - \ln\left(\frac{\eta}{\eta_b}\right) - \frac{11}{6}. \tag{A.6}$$

So, the full expression is

$$h(\eta) = \exp\left(-\frac{4\pi}{3}\frac{\Gamma_0}{H^4}\left[\frac{1}{3}(\frac{\eta}{\eta_b})^3 - \frac{3}{2}(\frac{\eta}{\eta_b})^2 + 3\frac{\eta}{\eta_b} - \ln\left(\frac{\eta}{\eta_b}\right) - \frac{11}{6}\right]\right). \tag{A.7}$$